

# RoboGaze: Evaluating Robot World Models via Structured Vision-Language Analysis

Minh-Loi Nguyen<sup>1</sup> Nghiem Tuong Diep<sup>2</sup> Hung Khang Nguyen<sup>2</sup> Minh Le<sup>2</sup>  
Doanh Le Thien<sup>1,2</sup> Hoang H. Tran<sup>1</sup> Dung Duy Le<sup>1</sup> Vu Duong<sup>1</sup> Daniel Sonntag<sup>3</sup>  
An Thai Le<sup>1,2,6</sup> Duy M. H. Nguyen<sup>3,4,5</sup> Ngo Anh Vien<sup>†1,2</sup> Tran Van Nhiem<sup>†2</sup>

<sup>1</sup>Center for AI Research, VinUniversity <sup>2</sup>VinRobotics <sup>3</sup>DFKI <sup>4</sup>University of Stuttgart

<sup>5</sup>Max Planck Research School for Intelligent Systems <sup>6</sup>Technische Universität Darmstadt

<sup>†</sup>Project Leads.

**Abstract:** Recent advances in robot world models enable synthetic video generation for embodied prediction and planning. However, evaluating these videos is challenging: visually realistic outputs often violate physical laws, temporal consistency, or task logic, while conventional metrics and monolithic Vision-Language Model (VLM) judges fail to generalize or provide precise diagnostic value. We present RoboGaze, a training-free, multi-agent VLM framework that provides structured, interpretable evaluation for generated robot-manipulation videos. Given a task instruction and video, RoboGaze operates via a three-stage pipeline: task-scene grounding, dimension-specific specialist routing, and critic-based verification. It outputs temporally localized glitch reports categorized under a novel 6-dimension, 30-type robotics-specific taxonomy. To benchmark RoboGaze, we introduce a human-validated dataset of 382 clips spanning simulated and real-world multi-view manipulation. Evaluating eight open-source and proprietary VLM backbones, RoboGaze dramatically outperforms zero-shot baselines, improving description- $F_1$  by up to +43 points and temporal alignment ( $F_1 \times \text{IoU}$ ) by up to +37 points – closing approximately 85% of the gap to the human ceiling. Furthermore, its critic verifier mitigates the “cry-wolf” false-positive flaw of standard VLMs, lifting clean-clip accuracy from under 25% to over 80%. RoboGaze offers a scalable, highly interpretable diagnostic tool for the rigorous evaluation of robot world models.

**Project webpage:** <https://robogaze-eval.github.io/>

**Keywords:** Robot world models, Manipulation video evaluation, Glitch diagnosis

## 1 Introduction

Recent advances in generative world models have made synthetic video a promising interface for embodied AI, enabling robot-centric rollouts for manipulation prediction, demonstration synthesis, and policy evaluation [1, 2, 3, 4, 5, 6, 7]. For robotics, however, visual realism alone is insufficient: generated videos must also be physically plausible, temporally coherent, and task-executable. Videos that look realistic yet violate physics, break temporal consistency, or fail the task are of limited value downstream, creating a fundamental gap between perceptual quality and robotics utility.

Existing evaluation methods do not adequately capture these requirements. Perceptual similarity metrics focus on low-level visual fidelity, while general video evaluation frameworks such as VBench [8], DOVER [9], and VideoScore [10] primarily assess overall video quality rather than execution correctness. Human evaluation [11] remains the most reliable approach, but is expensive, slow, and difficult to scale. Recent VLM-based evaluators [12, 13, 14] improve alignment with human judgments, while emerging world critics demonstrate strong reasoning capabilities for physical plausibility, common-sense consistency, and semantic correctness [15, 16, 17, 12]. However, existing approaches largely focus on holistic quality assessment and provide limited support for robotics-specific diagnosis, where identifying what failed, when it failed, why it failed, and how severe the failure is remains essential.

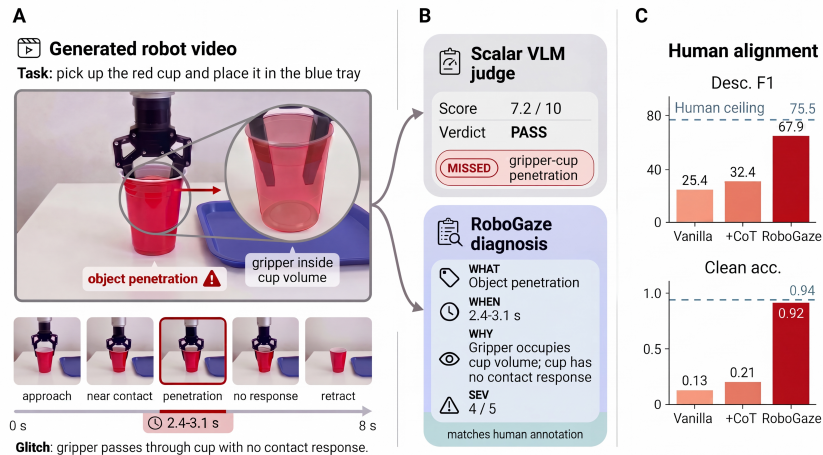


**Figure 1: RoboGaze vs. Monolithic VLM Judges.** While standard scalar evaluators fail to detect fine-grained physical anomalies like object penetration (A, B), RoboGaze delivers highly interpretable, temporally localized failure diagnostics, approaching the human ceiling on both description  $F_1$  and clean-clip accuracy (C).

To address this gap, we introduce **RoboGaze**, a training-free multi-agent VLM evaluator for robot video generation (Figure 1). RoboGaze is built around three key innovations: (i) *a robotics-specific glitch taxonomy comprising 6 evaluation dimensions and 30 failure types*; (ii) *subtask-level temporal grounding that localizes failures during task execution*, and (iii) *a verifier-based multi-agent reasoning framework that diagnoses, validates, and reports failures with interpretable evidence*. Rather than assigning a single quality score, RoboGaze reframes robot video evaluation as a structured reasoning problem over task progression, physical interactions, and execution correctness. To our knowledge, RoboGaze is the first evaluator that combines training-free evaluation, a robotics-specific taxonomy, and temporally localized diagnostic reporting within a unified framework.

To support rigorous evaluation, we construct a human-validated benchmark with temporally localized glitch annotations, severity labels, and free-text descriptions. Unlike prior benchmarks limited to video-level judgments, ours enables fine-grained failure localization under a structured robotics-specific taxonomy. Across multiple robot video generation settings, RoboGaze achieves the strongest agreement with human evaluation among open-source and proprietary VLM baselines, with substantially more accurate and interpretable localization.

In summary, we contribute four artifacts to the robot-video evaluation:

- **A robotics-specific glitch taxonomy.** We introduce a hierarchical  $6 \times 30$  taxonomy of robot-video failures spanning task execution, instruction consistency, object interactions, robot behavior, physical plausibility, and visual quality.
- **RoboGazeBench.** We construct a human-validated benchmark of 382 generated robot-manipulation videos with temporally localized glitch annotations, severity labels, and diagnostic descriptions across simulation and real-world domains.
- **RoboGaze.** We propose a training-free, model-agnostic multi-agent VLM evaluator that performs temporally grounded failure diagnosis and generates structured diagnostic reports instead of scalar quality scores.
- **Comprehensive empirical validation.** We evaluate RoboGaze across eight proprietary and open-source VLMs, demonstrating substantially stronger agreement with human judgments and more accurate failure localization than existing prompting and evaluation baselines.

## 2 Related Work

**Synthetic Video Generation and Robot World Models.** Large-scale video diffusion systems such as CogVideo [5] enable high-fidelity synthetic videos but prioritize visual quality over physical executability [25]. Cosmos-Predict [1, 7] unifies multi-modal world generation with better instruction following and physical consistency, while DreamGen [26] and DreamDojo [27] extend robot-centric

**Table 1:** Comparison of related video evaluation methods. The highlighted row marks the only training-free method that provides robotics-specific, temporally localized diagnostic reports with severity and grounded evidence.

Method	Focus	Temp. loc.	Diagnose	Severity	Grounded evidence	Robotics	Train-free	Output
VBench [8]	Gen. quality	No	No	No	No	No	Yes	Visual score
VideoScore [10]	Gen. quality	No	Limited	No	Limited	No	No	Multi-dim. score
WORLDJEN [14]	Multi-dim. eval.	No	Limited	No	Limited	No	Yes	Multi-dim. score
GRADEO [13]	Human-like eval.	No	Limited	Limited	Limited	No	No	Semantic score
VideoGen-Eval [18]	Structured eval.	Limited	Limited	No	Limited	No	Yes	Multi-dim. score
PAI-Bench [19]	Physical realism	No	Limited	No	Limited	Limited	Yes	Physics score
VideoHallu [20]	Hallucination	No	Yes	No	Limited	No	Yes	Hallu. report
GlitchBench [21]	Glitch detection	No	Yes	No	Limited	No	Yes	Glitch report
GLiDE [22]	Game glitch (open)	Yes	Yes	No	Limited	No	Yes	Glitch report
WorldSimBench [23]	World model eval.	No	Limited	No	Limited	Yes	No	Benchmark score
RBench [24]	Robot video eval.	No	Limited	No	Limited	Yes	Yes	Robotic score
RoboWM-Bench [17]	Robot exec. eval.	Limited	Limited	No	Limited	Yes	Limited	Exec. score
Morpheus [16]	Physical reasoning	No	Limited	No	Limited	Yes	Yes	Physics score
<b>RoboGaze</b>	<b>Robot diagnosis</b>	<b>Yes</b>	<b>Yes</b>	<b>Yes</b>	<b>Yes</b>	<b>Yes</b>	<b>Yes</b>	<b>Structured diagnostic report</b>

generation to zero-shot and dexterous tasks. These advances establish synthetic robot video as a practical embodied AI interface, but persistent failure modes – hallucinated physics and instruction-irrelevant rollouts – motivate evaluation beyond visual fidelity. Beyond basic evaluation, these generative world models hold immense potential for synthesizing targeted training data to robustify Vision-Language-Action (VLA) [28, 29] models in complex settings. Specifically, for long-horizon manipulation tasks prone to compounding execution errors [30, 31], world models can simulate multi-stage trajectories to pre-train policies on diverse action transitions. Similarly, by proceduralizing layout and asset variations, they can synthesize highly cluttered scenes [32] with varied occlusions and distractors. This allows VLAs to learn robust spatial reasoning and object persistence entirely through simulated data [33, 34, 35], bypassing the bottleneck of real-world data collection.

**General Evaluation of Generated Videos.** Traditional video metrics (e.g., PSNR, SSIM [36], LPIPS [37], FVD [38]) measure perceptual or distributional similarity but are insensitive to physics, temporal consistency, and task correctness. Structured benchmarks like VBench [8, 15, 9, 39] add multi-dimensional scoring, yet target *general realism* with holistic, video-level assessments rather than task-grounded diagnostics. Learned judges such as VideoScore and VideoScore2 [10, 12] score creative videos with VLMs, but demand large-scale supervision and operate at the coarse dimension level. Crucially, existing approaches lack the temporally localized failure diagnosis and execution reasoning required for robotics.

**VLM-Based Diagnostics and Physical Realism.** Recent VLM-based evaluators expand automatic video assessment into structured reasoning, evidence-based critiquing, and physical plausibility analysis [18, 14, 13, 40]. However, most rely on *monolithic VLM judges* that yield global judgments or scalar scores, offering little insight into the specific timing, cause, or severity of a failure. Physical realism benchmarks like PAI-Bench [19] introduce physical-failure taxonomies, but function primarily as fixed frameworks for global, model-level comparisons over predefined test distributions. Furthermore, frontier multimodal models remain unreliable for physics-sensitive, temporally grounded diagnosis [11]. While diagnostic methods like VideoHallu [20], GlitchBench [21], and the agentic open-ended detector GLiDE [22] localize event-level inconsistencies, they target general hallucinations or video-game glitches rather than embodied execution. In particular GLiDE, the closest agentic, temporally grounded glitch detector, assumes free-form game footage with no task instruction, subtask structure, or physical-executability criteria. In contrast, RoboGaze formulates robot video evaluation as a training-free, multi-agent diagnostic problem. Guided by a robotics-specific 30-type glitch taxonomy, it jointly analyzes task progress, scene interaction, and physical plausibility to output temporally localized glitch reports complete with severity metrics, grounding evidence, and verification.

**Robotics-Specific Video Evaluation.** Recent benchmarks evaluate robot video generation using structural consistency, physical plausibility, and action completeness (RBench [24]), or via simulation-action translation and conservation laws (RoboWM-Bench [17], Morpheus [16]). WorldSimBench [23] evaluates human preference and closed-loop success, but like other simulation-dependent methods cannot scale to offline, real-robot video evaluation. Fundamentally, existing frameworks *rank generative models* via aggregated scores rather than *diagnose individual videos*,

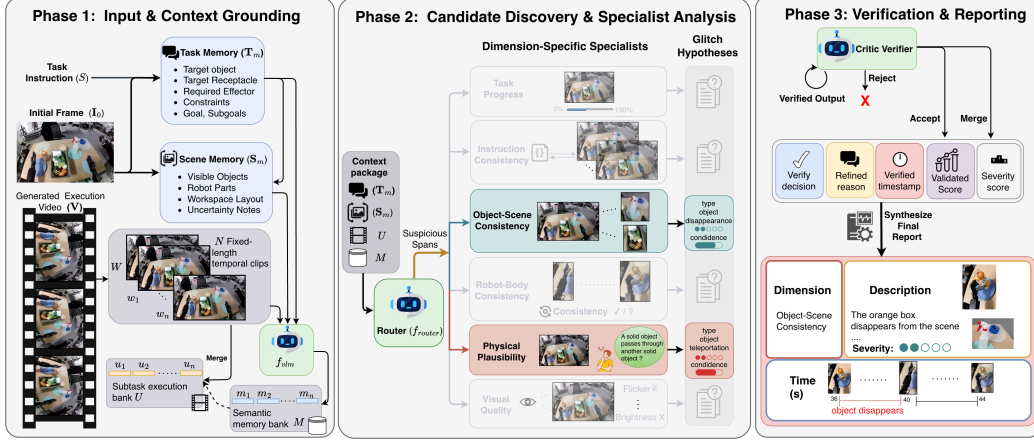


**Figure 2: The RoboGaze Framework.** A three-phase pipeline for video generation diagnosis: (1) extracting task and scene context memories; (2) routing suspicious temporal spans to six dimension-specific specialists to generate glitch hypotheses; and (3) verifying and synthesizing hypotheses into a final structured glitch report.

providing no per-video, temporally localized glitch annotations or diagnostic evidence. RoboGaze bridges these gaps: operating training-free and simulator-free, it delivers structured, per-video diagnostic reports with event-level temporal localization and severity-aware evidence.

### 3 Method

This section presents **RoboGaze**, a multi-agent framework for fine-grained evaluation of robot video generation. Given a task instruction, an optional initial scene observation, and a generated robot execution video, RoboGaze detects execution failures and produces structured diagnostic reports with failure types, supporting evidence, and likely causes. As shown in Figure 2, RoboGaze decomposes anomaly reasoning into three stages: (1) *Input and Context Grounding*, which builds task-grounded semantic memories from multimodal inputs; (2) *Candidate Discovery and Specialist Analysis*, where anomaly hypotheses are routed to specialized experts for diagnosis; and (3) *Verification and Reporting*, where a critic verifier validates findings and generates the final glitch report.

#### 3.1 Glitch Taxonomy.

We organize robot-video failures along a two-level taxonomy: 6 coarse *dimensions* that are each refined into a total of 30 fine-grained *types*. The six dimensions span the full execution stack of a manipulation rollout, from task semantics (*Task Progress, Instruction Consistency*), through object and robot dynamics (*Object-Scene, Robot-Body*), to physics and rendering (*Physical Plausibility, Visual Quality*). Specialist agents reason at the fine-grained type level; main-paper results aggregate at the dimension level. Full type definitions, the severity rubric, and the cascade rule are deferred to the appendix A.1.

#### 3.2 Input and Context Grounding

Given a task instruction  $S$ , an initial observation  $I_0$ , and a generated execution video  $V$ , RoboGaze first converts raw multimodal inputs into structured contextual memories for anomaly diagnosis. Directly prompting a VLM on long-horizon robot videos often yields weak temporal localization and ambiguous task reasoning amid large amounts of irrelevant visual context; RoboGaze therefore performs explicit task, scene, and temporal grounding first.

Specifically, RoboGaze parses  $S$  and  $I_0$  into a *task memory*  $T_m$ , encoding the global task objective and subtask-level specifications, including manipulated objects, target states, expected action outcomes, and completion criteria for each subtask. RoboGaze also constructs a *scene memory*  $S_m$  conditioned on  $T_m$  and  $I_0$ , representing the initial workspace configuration, visible objects, robot body parts, spatial relationships, and uncertainty cues from occlusion or ambiguous object states. Together,  $T_m$

and  $S_m$  provide semantic grounding for task intent and physical grounding for scene feasibility:

$$T_m = f_{\text{task}}(S, I_0), \quad S_m = f_{\text{scene}}(I_0, T_m), \quad (1)$$

where  $f_{\text{task}}$  and  $f_{\text{scene}}$  denote VLM-based semantic parsers for task and scene understanding.

To capture localized execution dynamics, RoboGaze decomposes  $V$  into  $N$  fixed-length temporal clips  $\mathcal{W} = \{w_1, \dots, w_N\}$ . Instead of directly localizing subtasks over the full video, RoboGaze converts localization into clip-level task-progress reasoning. Each clip is jointly analyzed with  $T_m$  and  $S_m$  to produce a structured semantic observation:

$$\mathcal{M} = \{m_i\}_{i=1}^N, \quad m_i = f_{\text{vlm}}(w_i, T_m, S_m), \quad (2)$$

where  $m_i$  summarizes robot actions, object state transitions, task progress signals, anomalies, and uncertainty cues within clip  $w_i$ . Using these progress signals, RoboGaze groups temporally related clips into subtask-specific execution segments:

$$\mathcal{U} = \{u_k\}_{k=1}^K, \quad u_k = \text{Merge}(\{w_i \mid i \in \mathcal{I}_k\}), \quad (3)$$

where  $\mathcal{I}_k$  denotes clips associated with subtask  $k$ , and  $\text{Merge}(\cdot)$  combines temporally contiguous clips into a unified sub-video.

The resulting package  $\mathcal{C} = \{T_m, S_m, \mathcal{M}, \mathcal{U}\}$  encodes task intent, scene conditions, localized execution evidence, and subtask-level temporal structure, enabling more reliable, temporally grounded reasoning than direct full-video prompting.

### 3.3 Candidate Discovery and Specialist Analysis

Given the context package  $\mathcal{C} = \{T_m, S_m, \mathcal{M}, \mathcal{U}\}$ , RoboGaze performs targeted diagnosis through sparse candidate routing and specialist analysis. Since only a subset of glitch dimensions is typically relevant to each subtask, applying all experts to every segment introduces noisy or weakly grounded diagnoses; RoboGaze therefore first identifies plausible failure dimensions before dispatching to relevant specialists.

For each subtask execution segment  $u_k \in \mathcal{U}$ , RoboGaze retrieves the corresponding task specification  $t_k \subset T_m$ , containing the expected objective and completion criteria for subtask  $k$ . A candidate router VLM then performs multi-label routing to predict a subset of plausible glitch dimensions:

$$G_k^{\text{cand}} = f_{\text{router}}(u_k, t_k), \quad G_k^{\text{cand}} \subseteq \mathcal{G}, \quad (4)$$

where  $\mathcal{G}$  denotes the six glitch dimensions and  $G_k^{\text{cand}}$  contains only dimensions likely relevant to the current execution segment. This routing mechanism improves diagnosis focus by restricting reasoning to task-relevant failure spaces.

For each candidate dimension  $g \in G_k^{\text{cand}}$ , the corresponding specialist performs fine-grained diagnosis conditioned on the execution segment, task specification, and scene grounding:

$$d_{k,g} = f_g(u_k, t_k, S_m) = (y_{k,g}, r_{k,g}, \tau_{k,g}, e_{k,g}, \tilde{s}_{k,g}, c_{k,g}), \quad (5)$$

where  $y_{k,g} \in \{0, 1\}$  indicates whether a glitch is detected,  $r_{k,g}$  provides diagnostic reasoning,  $\tau_{k,g}$  localizes the glitch temporally,  $e_{k,g}$  summarizes supporting evidence,  $\tilde{s}_{k,g}$  is a proposed severity, and  $c_{k,g}$  is the confidence score.

Aggregating all specialist diagnoses yields  $\mathcal{D} = \{d_{k,g} \mid g \in G_k^{\text{cand}}, k = 1, \dots, K\}$ , a structured set of anomaly hypotheses for verification. Combining sparse routing with dimension-specific specialists yields fine-grained, temporally localized, evidence-grounded diagnosis without exhaustive analysis over all dimensions.

### 3.4 Verification and Reporting

The Stage-2 diagnoses  $\mathcal{D}$  are candidate hypotheses that may still be uncertain, weakly grounded, or redundant across dimensions. RoboGaze therefore adjudicates the hypothesis set as a whole:

validating supported claims, suppressing unsupported ones, and consolidating duplicates into a single coherent report.

A critic verifier re-examines each hypothesis  $d_{k,g} \in \mathcal{D}$  against the execution segment, diagnostic reasoning, temporal localization, supporting evidence, and task–scene grounding, and assigns one of three actions:

$$f_{\text{verify}}(d_{k,g}, u_k, t_k, S_m) \rightarrow a_{k,g} \in \{\text{ACCEPT}, \text{REJECT}, \text{MERGE}\}. \quad (6)$$

A hypothesis is **ACCEPTED** if it is visually supported, temporally consistent, and semantically aligned with task and scene constraints; **REJECTED** if its evidence is better explained by normal execution (e.g., occlusion rather than object disappearance); and **MERGED** when it describes the same physical event as another – matching object or action, overlapping span, and consistent evidence – in which case the group is consolidated under a single primary dimension and type. Independent failures stay separate even when their spans overlap. Each surviving hypothesis is returned as  $\hat{d}_{k,g} = (\hat{r}_{k,g}, \hat{t}_{k,g}, \hat{e}_{k,g}, s_{k,g})$  with a refined explanation, verified span, validated evidence, and validated severity. Aggregating the accepted and merged hypotheses yields  $\hat{\mathcal{D}}$ , synthesized into the final report  $R = f_{\text{report}}(\hat{\mathcal{D}})$ . By contesting specialist hypotheses before they enter the report, this stage sharply reduces false positives and drives RoboGaze’s clean-clip reliability (Section 4.3).

## 4 Experiments

### 4.1 Setup and Annotation

**Benchmark.** ROBOGAZEBENCH contains 382 generated robot-manipulation clips spanning simulated GR-1 tasks (**GR1-Sim**), real-initialized GR-1 tasks (**GR1-Real**), and real-domain multi-view manipulation clips (**DROID-MV**); Table 2 summarizes the three splits. These splits test whether diagnostic evaluation transfers across domain realism and camera configuration; dataset construction details and source citations are deferred to the appendix A.2.

Dataset	Clips	Domain	View	Avg. dur.
GR1-Sim	154	Sim	Single	8–9 s
GR1-Real	100	Real-init	Single	5–6 s
DROID-MV	128	Real	Multi	17–18 s
<b>Total</b>	<b>382</b>	–	–	–

**Table 2:** Summary of the three ROBOGAZEBENCH evaluation splits.

**Models and conditions.** We evaluate eight vision–language backbones spanning proprietary models (**Gemini 3.1 Pro** [41], **GPT-5.5** [42], **Gemini 3.1 Flash** [41], **Claude Sonnet 4.6**) and open-source models (**Gemma4-31B** [43], **Qwen3.6-35B** [44, 45], **LLaVA-OneVision-2-8B-Instruct** [46], **InternVL3.5-38B** [47]). Each backbone is tested in three conditions: zero-shot **vanilla**, **+CoT**, and wrapped by **ROBOGAZE (+RG)**, with the visual-input regime fixed across conditions; prompts, serving details, and sampling ablations are in the appendix A.3 and A.4.

**Human annotations.** Each clip is annotated *from scratch* by two robotics-trained annotators and adjudicated by a senior annotator, who see only the generated video and task instruction; for each event we record its dimension, type, temporal span, severity, and free-form description. A 60-video gold subset (20 per split) is independently labeled by three senior annotators to estimate reliability and the human ceiling. The annotation guide, interface, and adjudication rules are in the appendix A.2.

Agreement is strong across all five metrics (Table 3); DROID-MV is slightly harder due to longer, multi-view-grid clips. We use the gold subset to estimate a human ceiling, evaluating each annotator against the consensus of the other two (the *Human (ceiling)* row in Table 4).

### 4.2 Evaluation Protocol

We adopt the open-ended matching protocol of GLiDE [22], scoring each predicted report by globally matching predicted and reference events using both semantic agreement and temporal overlap. For video  $v$ , let predictions be  $\mathcal{P}_v = \{p_i\}_{i=1}^N$  and references be  $\hat{\mathcal{Y}}_v = \{\hat{y}_j\}_{j=1}^M$ , where each event contains a dimension, type, temporal span, severity, and description. A fixed LLM judge assigns description similarity  $S_{ij} \in [0, 1]$  for each prediction–reference pair using a rubric over event faithfulness,

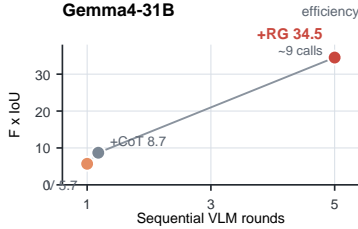


**Figure 3:** Gemma4-31B efficiency trade-off. Points are vanilla, +CoT, and +RG; labels show VLM calls/video.

**Table 3:** Inter-annotator agreement on the 60-video gold subset. Metrics cover clip-level detection, event dimension, temporal span, ordinal severity, and free-text diagnostic agreement; higher is better for all metrics.

Metric $\uparrow$	GR1-Sim	GR1-Real	DROID-MV	Overall
Detection $\kappa$ (per clip)	0.82	0.79	0.71	0.77
Dimension $\kappa$ (per event)	0.74	0.70	0.63	0.69
Mean pairwise temporal IoU	0.68	0.65	0.58	0.64
Severity Krippendorff’s $\alpha$ (ordinal)	0.66	0.62	0.55	0.61
Description sim. (LLM judge, 0-1)	0.79	0.76	0.71	0.75

specificity, and causal correctness. We then score each pair as the product of three interpretable factors – description similarity, temporal overlap, and a dimension-agreement bonus:

$$C_{ij} = S_{ij} \cdot \text{IoU}_t(\tau_i, \hat{\tau}_j) \cdot \beta_{ij}, \quad \beta_{ij} = 1 + \lambda_{\text{dim}} \mathbb{1}[\text{dim}_i = \hat{\text{dim}}_j], \quad (7)$$

where  $\tau_i$  and  $\hat{\tau}_j$  are the predicted and reference temporal spans,  $\text{IoU}_t$  is their temporal intersection-over-union, and the bonus  $\beta_{ij}$  rewards dimension agreement with  $\lambda_{\text{dim}} = 0.25$ . Maximum-weight Hungarian assignment [48] over  $C$  gives the one-to-one matched set  $\mathcal{A}$ .

We report description precision/recall/ $F_1$  by summing  $S_{ij}$  over  $\mathcal{A}$  and normalizing by  $N$  or  $M$ , temporal mIoU by averaging  $\text{IoU}_t$  over matched pairs, and joint  $F_1 \times \text{IoU}$  by replacing  $S_{ij}$  with  $S_{ij} \text{IoU}_t$  in the same precision–recall computation. We additionally report severity within-1 accuracy on matched events and clean-clip accuracy for no-glitch videos, which captures the false-positive behavior of monolithic judges. Judge prompts, thresholded temporal metrics, severity-weighted scores, per-dataset breakdowns, and loose-matching variants are in the appendix.

### 4.3 Main Results

**Table 4:** Main results on ROBOGAZEBENCH, averaged across the three datasets. V, CoT, and RG denote vanilla prompting, chain-of-thought prompting, and the same backbone wrapped by ROBOGAZE; shaded RG columns show the primary comparison. Higher is better for all metrics, and Clean is clean-clip accuracy.

Family	Model	Desc. $F_1 \uparrow$			mIoU $\uparrow$			$F \times \text{IoU} \uparrow$			Clean $\uparrow$		
		V	CoT	RG	V	CoT	RG	V	CoT	RG	V	CoT	RG
Prop.	Gemini 3.1 Pro	25.4	32.4	<b>67.9</b>	.39	.43	<b>.64</b>	9.8	13.9	<b>43.7</b>	.13	.21	<b>.92</b>
	GPT-5.5	23.9	30.5	<b>65.1</b>	.37	.41	<b>.63</b>	8.8	12.5	<b>41.1</b>	.09	.18	<b>.90</b>
	Gemini 3.1 Flash	20.2	26.1	<b>57.8</b>	.35	.39	<b>.61</b>	7.0	10.2	<b>35.0</b>	.08	.16	<b>.87</b>
	Claude Sonnet 4.6	21.4	27.6	<b>60.3</b>	.36	.40	<b>.61</b>	7.7	11.0	<b>36.8</b>	.11	.20	<b>.89</b>
Open	Gemma4-31B	17.6	23.4	<b>56.6</b>	.33	.37	<b>.66</b>	5.7	8.7	<b>34.5</b>	.03	.12	<b>.86</b>
	Qwen3.6-35B	16.7	22.3	<b>53.1</b>	.32	.36	<b>.60</b>	5.4	8.2	<b>31.6</b>	.16	.23	<b>.84</b>
	LLaVA-OV-2-8B	14.2	19.5	<b>47.9</b>	.30	.33	<b>.56</b>	4.3	6.5	<b>26.9</b>	.18	.25	<b>.82</b>
	InternVL3.5-38B	15.5	21.0	<b>50.1</b>	.31	.35	<b>.58</b>	4.8	7.4	<b>28.9</b>	.04	.13	<b>.81</b>
Human	ceiling	75.5			0.71			47.1			0.94		

Table 4 reports the headline comparison on ROBOGAZEBENCH, averaged across the three datasets. Three findings stand out.

**(i) Monolithic VLM judges are brittle for robot-video diagnosis.** Vanilla VLMs often recognize suspicious motion but do not reliably decide whether it constitutes a task-relevant, physically grounded failure. Chain-of-thought prompting improves consistency but does not resolve the central failure mode: without task–scene grounding and explicit evidence checks, models convert uncertainty or unusual-but-valid motion into false glitch reports.

**(ii) ROBOGAZE improves diagnostic agreement across model families.** Wrapping the same backbone with ROBOGAZE consistently improves semantic agreement, temporal localization, and the joint score across both proprietary and open-source models, indicating the improvement comes from evaluator structure rather than backbone scale alone. The per-dimension breakdown (Figure 4) shows the largest gains on Task Progress, Instruction Consistency, Object–Scene, and Robot–Body failures, where diagnosis depends on relational and causal reasoning.

**(iii) The critic verifier addresses the cry-wolf failure mode.** The key difference between ROBOGAZE and monolithic judges is not that it proposes more candidate glitches, but that it rejects weak ones: the verifier checks each hypothesis against visual evidence, task context, scene state, and temporal consistency before it enters the report. This explains the large clean-clip improvement and is consistent with the ablation (Table 5), where removing the verifier causes the largest degradation; Figure 5 shows representative cases, including a false positive the verifier rejects (b).

#### 4.4 Ablation Studies

Table 5 ablates ROBOGAZE’s structural components on Gemma4-31B: every component contributes, but removing the critic verifier causes the largest degradation, supporting our central claim that reliable robot-video evaluation needs both structured context and an explicit mechanism for rejecting weak hypotheses. These gains carry a higher inference cost; Figure 3 plots the accuracy–compute trade-off across the vanilla, +CoT, and +RG conditions. More detail about cost and runtime are shown in ablation A.4.9

**Judge robustness.** Re-evaluating Table 4 with an alternate LLM judge preserves model rankings and yields highly correlated scores, indicating the trends are not an artifact of a single judge model; full correlations, score differences, and judge prompts are in the appendix A.4.

#### 4.5 Qualitative Analysis

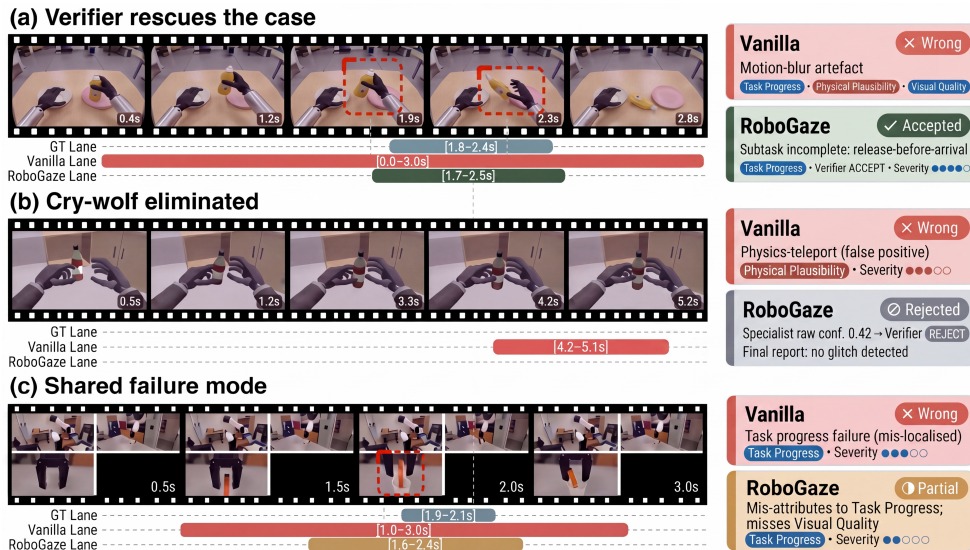


**Figure 5:** Qualitative comparison between vanilla baselines and ROBOGAZE on three representative clips: (a) the verifier rescues a true glitch a vanilla judge mislabels, (b) a vanilla false positive is rejected, and (c) a failure both methods detect but localize differently.

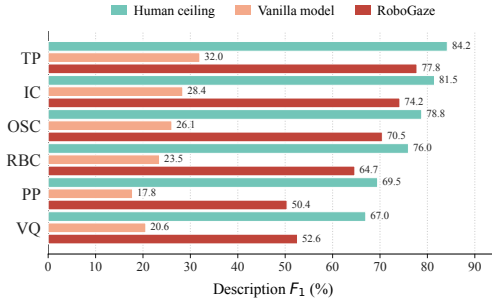


**Figure 4:** Per-dimension description- $F_1$  for Gemini 3.1 Pro on ROBOGAZEBENCH, averaged across the three datasets. Description- $F_1$  measures the agreement between predicted and human diagnostic descriptions within each glitch dimension; higher is better.

Configuration	Desc. $F_1$ $\uparrow$	mIoU $\uparrow$	$F \times IoU$ $\uparrow$	Sev@1 $\uparrow$
ROBOGAZE (Gemma4-31B)	<b>56.6</b>	<b>0.66</b>	<b>34.5</b>	<b>81.4</b>
w/o task memory	51.2	0.61	29.2	76.8
w/o scene memory	50.0	0.60	28.3	75.9
w/o subtask segmentation	52.7	0.62	30.6	77.5
w/o candidate router	51.5	0.63	30.8	77.0
w/o critic verifier	44.3	0.59	23.8	71.7

**Table 5:** Ablation of Gemma4-31B with ROBOGAZE, averaged across the three datasets. The shaded full-system row is the reference; the shaded verifier ablation marks the largest degradation.

## 5 Conclusion

We presented ROBOGAZE, a training-free, model-agnostic evaluator that turns monolithic VLM judges into temporally localized robot-video diagnosticians. Across three benchmark splits and eight VLM backbones, evaluator *structure* – task–scene grounding, routed specialists, and critic verification – is the main driver of reliable diagnostic agreement. We view structured glitch reports as a complement to scalar preference signals for offline benchmarking, dataset curation, and closed-loop world-model development.

**Limitations.** Several limitations remain. The residual human gap concentrates on *Physical Plausibility* and *Visual Quality*, which likely need explicit 3D geometry or pixel-level signals (e.g., optical flow) rather than text-based prompting. ROBOGAZEBENCH also draws from a single generator family, so broader claims need wider coverage of embodiments, camera layouts, and architectures. Finally, our view-agnostic specialists can miss view-dependent evidence, the precision-oriented verifier can suppress rare transient glitches (leaving the precision–recall point downstream-dependent), and the closed-world taxonomy with multi-agent orchestration costs more than a monolithic judge.

## References

- [1] A. Ali, J. Bai, M. Bala, Y. Balaji, A. Blakeman, T. Cai, J. Cao, T. Cao, E. Cha, Y.-W. Chao, et al. World simulation with video foundation models for physical ai. *arXiv preprint arXiv:2511.00062*, 2025.
- [2] A. Hu, L. Russell, H. Yeo, Z. Murez, G. Fedoseev, A. Kendall, J. Shotton, and G. Corrado. Gaia-1: A generative world model for autonomous driving. *arXiv preprint arXiv:2309.17080*, 2023.
- [3] J. Bruce, M. D. Dennis, A. Edwards, J. Parker-Holder, Y. Shi, E. Hughes, M. Lai, A. Mavalankar, R. Steigerwald, C. Apps, et al. Genie: Generative interactive environments. In *Forty-first International Conference on Machine Learning*, 2024.
- [4] Z. Yang, Y. Chen, J. Wang, S. Manivasagam, W.-C. Ma, A. J. Yang, and R. Urtasun. Unisim: A neural closed-loop sensor simulator. In *Proceedings of the IEEE/CVF Conference on Computer Vision and Pattern Recognition*, pages 1389–1399, 2023.
- [5] W. Hong, M. Ding, W. Zheng, X. Liu, and J. Tang. Cogvideo: Large-scale pretraining for text-to-video generation via transformers. In *The Eleventh International Conference on Learning Representations*.
- [6] D. M. Nguyen, N. T. Diep, B. G. Nguyen, T.-B. Ho, D. Le, T. Nguyen, T.-L. Ha, T. Nhiem, B. Thach, N. Tran, T. A. Tran, A. Habuda, P. L. Moeller, T. N. Le, D. Sonntag, M. Niepert, K. Doan, V. Doan, V. Duong, H. Ngo, M. Vu, D. M. Nguyen, A. T. Le, and V. Ngo. FOCA: Future-oriented conditioning for data-efficient vision-language-action adaptation. In *Proceedings of the International Conference on Machine Learning (ICML)*, 2026.
- [7] N. Agarwal, A. Ali, J. Allen, M. Antolini, A. Aubame, J. Azzolini, J. Bai, M. Bala, Y. Balaji, J. Bapst, et al. Cosmos 3: Omnimodal world models for physical ai. *arXiv preprint arXiv:2606.02800*, 2026. doi:10.48550/arXiv.2606.02800. URL <https://arxiv.org/abs/2606.02800>.
- [8] Z. Huang, Y. He, J. Yu, F. Zhang, C. Si, Y. Jiang, Y. Zhang, T. Wu, Q. Jin, N. Chanpaisit, et al. Vbench: Comprehensive benchmark suite for video generative models. In *Proceedings of the IEEE/CVF Conference on Computer Vision and Pattern Recognition*, pages 21807–21818, 2024.
- [9] H. Wu, E. Zhang, L. Liao, C. Chen, J. Hou, A. Wang, W. Sun, Q. Yan, and W. Lin. Exploring video quality assessment on user generated contents from aesthetic and technical perspectives. In

- Proceedings of the IEEE/CVF international conference on computer vision*, pages 20144–20154, 2023.
- [10] X. He, D. Jiang, G. Zhang, M. Ku, A. Soni, S. Siu, H. Chen, A. Chandra, Z. Jiang, A. Arulraj, et al. Videoscore: Building automatic metrics to simulate fine-grained human feedback for video generation. In *Proceedings of the 2024 Conference on Empirical Methods in Natural Language Processing*, pages 2105–2123, 2024.
- [11] Q. Zhang, P. Jing, H.-X. Yu, F. Ding, F. Nie, W. Wang, Y. Du, J. Zou, J. Wu, and B. Shuai. Physion-eval: Evaluating physical realism in generated video via human reasoning. *arXiv preprint arXiv:2603.19607*, 2026.
- [12] X. He, D. Jiang, P. Nie, M. Liu, Z. Jiang, M. Su, W. Ma, J. Lin, C. Ye, Y. Lu, et al. Videoscore2: Think before you score in generative video evaluation. *arXiv preprint arXiv:2509.22799*, 2025.
- [13] Z. Mou, B. Xia, Z. Huang, W. Yang, and J. Jia. Gradeo: Towards human-like evaluation for text-to-video generation via multi-step reasoning. In *International Conference on Machine Learning*, pages 44971–44996. PMLR, 2025.
- [14] K. Inbasekar, G. Rom, and O. Shlomovits. Worldjen: An end-to-end multi-dimensional benchmark for generative video models. *arXiv preprint arXiv:2605.03475*, 2026.
- [15] D. Zheng, Z. Huang, H. Liu, K. Zou, Y. He, F. Zhang, L. Gu, Y. Zhang, J. He, W.-S. Zheng, et al. Vbench-2.0: Advancing video generation benchmark suite for intrinsic faithfulness. *arXiv preprint arXiv:2503.21755*, 2025.
- [16] C. Zhang, D. Cherniavskii, A. Tragoudaras, A. Vozikis, T. Nijdam, D. W. Prinzhorn, M. Bodrac-ska, N. Sebe, A. Zadaianchuk, and E. Gavves. Morpheus: Benchmarking physical reasoning of video generative models with real physical experiments. *arXiv preprint arXiv:2504.02918*, 2025.
- [17] F. Jiang, Y. Chen, K. Xu, Y. Liu, H. Wang, Z. Shen, J. Lu, S. Huang, Y. Wang, C. Xie, et al. Robowm-bench: A benchmark for evaluating world models in robotic manipulation. *arXiv preprint arXiv:2604.19092*, 2026.
- [18] Y. Yang, K. Fan, S. Sun, H. Li, A. Zeng, F. Han, W. Zhai, W. Liu, Y. Cao, and Z.-J. Zha. Videogen-eval: Agent-based system for video generation evaluation. *arXiv preprint arXiv:2503.23452*, 2025.
- [19] F. Zhou, J. Huang, J. Li, D. Ramanan, and H. Shi. Pai-bench: A comprehensive benchmark for physical ai, 2025. URL <https://arxiv.org/abs/2512.01989>.
- [20] Z. Li, X. Wu, G. Shi, Y. Qin, H. Du, T. Zhou, D. Manocha, and J. Boyd-Graber. Video-hallu: Evaluating and mitigating multi-modal hallucinations on synthetic video understanding. *Advances in Neural Information Processing Systems*, 38:76046–76078, 2026.
- [21] M. R. Taesiri, T. Feng, C.-P. Bezemer, and A. Nguyen. Glitchbench: Can large multimodal models detect video game glitches? In *Proceedings of the IEEE/CVF Conference on Computer Vision and Pattern Recognition*, pages 22444–22455, 2024.
- [22] M. Zheng, T. Zhou, G. Wu, Z. Lin, H. Wang, and L. Huang. Open-ended video game glitch detection with agentic reasoning and temporal grounding. *arXiv preprint arXiv:2604.07818*, 2026.
- [23] Y. Qin, Z. Shi, J. Yu, X. Wang, E. Zhou, L. Li, Z. Yin, X. Liu, L. Sheng, J. Shao, et al. Worldsim-bench: Towards video generation models as world simulators. *arXiv preprint arXiv:2410.18072*, 2024.
- [24] Y. Deng, Z. Pan, H. Zhang, X. Li, R. Hu, Y. Ding, Y. Zou, Y. Zeng, and D. Zhou. Rethinking video generation model for the embodied world. *arXiv preprint arXiv:2601.15282*, 2026.

- [25] Y. Wang, X. Liu, W. Pang, L. Ma, S. Yuan, P. Debevec, and N. Yu. Survey of video diffusion models: Foundations, implementations, and applications. *Transactions on Machine Learning Research*.
- [26] J. Jang, S. Ye, Z. Lin, J. Xiang, J. Bjorck, Y. Fang, F. Hu, S. Huang, K. Kundalia, Y.-C. Lin, et al. Dreamgen: Unlocking generalization in robot learning through video world models. In *Conference on Robot Learning*, pages 5170–5194. PMLR, 2025.
- [27] S. Gao, W. Liang, K. Zheng, A. Malik, S. Ye, S. Yu, W.-C. Tseng, Y. Dong, K. Mo, C.-H. Lin, et al. Dreamdojo: A generalist robot world model from large-scale human videos. *arXiv preprint arXiv:2602.06949*, 2026.
- [28] M. J. Kim, K. Huang, H. Gu, A. Shah, R. Torne, A. Sharma, K. Keetha, F. Ebert, S. Levine, and C. Finn. OpenVLA: An open-source vision-language-action model. In *Conference on Robot Learning (CoRL)*, 2024. URL <https://openvla.github.io>.
- [29] A. Brohan, N. Brown, J. Carbajal, Y. Chebotar, X. Chen, K. Choromanski, T. Ding, D. Danny, A. Fu, S. Guadarrama, et al. RT-2: Vision-language-action models transfer web knowledge to robotic control. *Conference on Robot Learning (CoRL)*, 2023. URL <https://arxiv.org/abs/2307.15818>.
- [30] N. Chung, T. Hanyu, T. Nguyen, H. Le, F. Bumgarner, D. M. Nguyen, K. Vo, K. I. Yamazaki, C. Rainwater, T. Kieu, A. Nguyen, and N. Le. Rethinking progression of memory state in robotic manipulation: An object-centric perspective. In *Proceedings of the AAAI Conference on Artificial Intelligence*, 2026.
- [31] T. Hanyu, N. Chung, H. Le, T. Nguyen, Y. Ikebe, A. Gunderman, D. M. H. Nguyen, K. Vo, T. Kieu, K. Yamazaki, C. Rainwater, A. Nguyen, and N. Le. SlotVLA: Towards modeling of object-relation representations in robotic manipulation. In *IEEE International Conference on Robotics and Automation (ICRA)*, 2026.
- [32] K. Vo, T. Hanyu, Y. Ikebe, T. T. Pham, N. Chung, M. N. Vu, D. M. H. Nguyen, A. Nguyen, A. Gunderman, C. Rainwater, and N. Le. Clutter-resistant vision–language–action models through object-centric and geometry grounding. *arXiv preprint arXiv:2512.22519*, 2026. URL <https://arxiv.org/abs/2512.22519>.
- [33] D. M. Nguyen, B.-N. Dao, T. M. Luu, B. G. Nguyen, V. Tong, A. Liu, V. N. Duong, D. D. Le, D. Sonntag, T. Le, N. Le, J. Peter, A. T. Le, M. N. Vu, M. Niepert, K. D. Doan, D. M. H. Nguyen, and V. A. Ngo. Self-improving VLA policies: Selected diffusion noise for spurious-robust action smoothing. *arXiv preprint arXiv:2606.14084*, 2026. URL <https://arxiv.org/abs/2606.14084>.
- [34] A. Authors. Ctrl-world: A controllable generative world model for robot manipulation. *arXiv preprint arXiv:2510.10125*, 2025. URL <https://arxiv.org/abs/2510.10125>.
- [35] A. Authors. Closed-loop learning of video world model and VLA policy. *arXiv preprint arXiv:2602.06508*, 2026. URL <https://arxiv.org/abs/2602.06508>.
- [36] Z. Wang, A. C. Bovik, H. R. Sheikh, and E. P. Simoncelli. Image quality assessment: from error visibility to structural similarity. *IEEE transactions on image processing*, 13(4):600–612, 2004.
- [37] R. Zhang, P. Isola, A. A. Efros, E. Shechtman, and O. Wang. The unreasonable effectiveness of deep features as a perceptual metric. In *Proceedings of the IEEE conference on computer vision and pattern recognition*, pages 586–595, 2018.
- [38] T. Unterthiner, S. Van Steenkiste, K. Kurach, R. Marinier, M. Michalski, and S. Gelly. Towards accurate generative models of video: A new metric & challenges. *arXiv preprint arXiv:1812.01717*, 2018.

- [39] H. Han, S. Li, J. Chen, Y. Yuan, Y. Wu, Y. Deng, C. T. Leong, H. Du, J. Fu, Y. Li, et al. Video-bench: Human-aligned video generation benchmark. In *Proceedings of the Computer Vision and Pattern Recognition Conference*, pages 18858–18868, 2025.
- [40] Y. Qi, Y. Zhao, Y. Zeng, X. Bao, W. Huang, L. Chen, Z. Chen, J. Zhao, Z. Qi, and F. Zhao. Vcr-bench: A comprehensive evaluation framework for video chain-of-thought reasoning. *arXiv preprint arXiv:2504.07956*, 2025.
- [41] G. Team, R. Anil, S. Borgeaud, J.-B. Alayrac, J. Yu, R. Soricut, J. Schalkwyk, A. M. Dai, A. Hauth, K. Millican, et al. Gemini: a family of highly capable multimodal models. *arXiv preprint arXiv:2312.11805*, 2023.
- [42] A. Singh, A. Fry, A. Perelman, A. Tart, A. Ganesh, A. El-Kishky, A. McLaughlin, A. Low, A. Ostrow, A. Ananthram, et al. Openai gpt-5 system card. *arXiv preprint arXiv:2601.03267*, 2025.
- [43] G. Team, T. Mesnard, C. Hardin, R. Dadashi, S. Bhupatiraju, S. Pathak, L. Sifre, M. Rivière, M. S. Kale, J. Love, et al. Gemma: Open models based on gemini research and technology. *arXiv preprint arXiv:2403.08295*, 2024.
- [44] S. Bai, Y. Cai, R. Chen, K. Chen, X. Chen, Z. Cheng, L. Deng, W. Ding, C. Gao, C. Ge, et al. Qwen3-vl technical report. *arXiv preprint arXiv:2511.21631*, 2025.
- [45] A. Yang, A. Li, B. Yang, B. Zhang, B. Hui, B. Zheng, B. Yu, C. Gao, C. Huang, C. Lv, et al. Qwen3 technical report. *arXiv preprint arXiv:2505.09388*, 2025.
- [46] B. Li, Y. Zhang, D. Guo, R. Zhang, F. Li, H. Zhang, K. Zhang, P. Zhang, Y. Li, Z. Liu, et al. Llava-onevision: Easy visual task transfer. *arXiv preprint arXiv:2408.03326*, 2024.
- [47] W. Wang, Z. Gao, L. Gu, H. Pu, L. Cui, X. Wei, Z. Liu, L. Jing, S. Ye, J. Shao, et al. Internvl3. 5: Advancing open-source multimodal models in versatility, reasoning, and efficiency. *arXiv preprint arXiv:2508.18265*, 2025.
- [48] H. W. Kuhn. The hungarian method for the assignment problem. *Naval research logistics quarterly*, 2(1-2):83–97, 1955.
- [49] A. Khazatsky, K. Pertsch, S. Nair, A. Balakrishna, S. Dasari, S. Karamcheti, S. Nasiriany, M. K. Srirama, L. Y. Chen, K. Ellis, et al. Droid: A large-scale in-the-wild robot manipulation dataset. *arXiv preprint arXiv:2403.12945*, 2024.

A	Appendix	13
A.1	Glitch Taxonomy	13
A.2	Experimental Details	13
A.3	Prompts	19
A.4	Robustness and Diagnostic Analyses	22

## A.1 Glitch Taxonomy

**Summary.** Table 6 shows the full 6-dimension  $\times$  30-type glitch taxonomy used by the benchmark, specialist agents, and per-dimension analyses.

**Severity rubric.** Each annotated event additionally carries an ordinal severity score in  $\{1, 2, 3, 4, 5\}$ : 1 = cosmetic (visible artifact but task state and object interaction remain interpretable); 2 = minor (localized failure with little ambiguity about the intended execution); 3 = moderate (failure affects an object, robot part, or subtask transition that is relevant to the task); 4 = severe (failure obscures whether the task was executed correctly or would make the clip unsuitable as a clean demonstration); 5 = catastrophic (the clip depicts a physically or semantically impossible event that invalidates the task execution). We intentionally define severity using observable task-video properties rather than unmeasured downstream policy outcomes.

**Cascade rule for multi-dimensional events.** A single event is allowed to belong to multiple dimensions when its supporting evidence equally implicates more than one (e.g., a gripper passing through a cup is both a physical-plausibility and a robot-body event). Annotators apply the following cascade: assign all applicable dimensions, then promote the primary dimension based on the most directly observable evidence. Matching at the dimension level uses the primary dimension; the secondary dimensions are preserved internally for downstream analyses.

**Taxonomy and rubric independence.** To avoid circularity between the evaluation target and ROBOGAZE’s outputs, the taxonomy, severity rubric, and annotation guide were frozen before production annotation and before any model-generated reports were shown to annotators. Annotators never saw ROBOGAZE, vanilla, or +CoT outputs while labeling ROBOGAZEBENCH; model outputs are used only after adjudicated human references are finalized.

**Open-world residual audit.** During adjudication, senior annotators flagged events whose cause was ambiguous or cascading across multiple taxonomy dimensions. These cases were retained with primary and secondary dimensions rather than discarded. In the final benchmark, 21/382 clips (5.5%) contain at least one cascading event, and all could be mapped to an existing primary dimension plus optional secondary dimensions. We therefore treat the taxonomy as closed-world for scoring, while preserving secondary labels to support future open-world analyses.

## A.2 Experimental Details

**Summary.** Reproducibility details for dataset construction, annotation, the LLM judge, and per-backbone serving.

### A.2.1 Dataset Construction

**GR1-Sim.** We construct GR1-Sim from the NVIDIA PhysicalAI Robotics GR00T Teleop-Sim dataset<sup>1</sup>. We select the first 10 task families and sample 1,000 teleoperation trajectories, which are re-simulated in Isaac Sim to obtain egocentric humanoid-perspective RGB videos (resolution, FPS, and

<sup>1</sup><https://huggingface.co/datasets/nvidia/PhysicalAI-Robotics-GR00T-Teleop-Sim>. Hugging Face dataset card.

**Table 6:** Two-level RoboGaze glitch taxonomy: 6 dimensions and 30 fine-grained types. The dimension level is used for all per-dimension analyses in the main paper; the fine-grained type level is used by specialist agents during diagnosis and by annotators for event-level labels.

Dimension	Fine-grained type	Definition
<b>Task Progress (TP)</b>	task_incompletion	The task is attempted but the required final state is not reached.
	failed_grasp	The robot attempts to grasp an object but never establishes a stable grasp.
	failed_placement	The robot transports or manipulates an object but fails to place it in the intended final state.
	premature_termination	The episode ends before the task-relevant action sequence is complete.
	ambiguous_task_success	The final state is visually ambiguous, making task success impossible to determine reliably.
<b>Instruction Consistency (IC)</b>	wrong_effector	The robot uses an effector inconsistent with the instruction or expected embodiment.
	wrong_object	The robot interacts with an object different from the one specified.
	wrong_target_location	The object is moved to a location inconsistent with the instruction.
	wrong_action_order	Required actions occur in an order inconsistent with the instruction.
<b>Object-Scene Consistency (OSC)</b>	ignored_instruction_constraint	A stated constraint, precondition, or task-specific requirement is ignored.
	object_hallucination	A new task-relevant object appears without a physically supported cause.
	object_disappearance	A visible object vanishes without being moved out of view or plausibly occluded.
	object_identity_swap	One object changes semantic identity or is replaced by another object.
	object_distortion	An object’s geometry deforms in a way inconsistent with its expected rigidity or articulation.
<b>Robot-Body Consistency (RBC)</b>	object_color_or_shape_drift	An object’s color, shape, or visual identity drifts over time without task-relevant cause.
	hallucinated_robot_part	A robot limb, gripper, finger, or body segment appears without physical continuity.
	missing_robot_part	A visible robot part disappears or becomes absent when it should remain visible.
	duplicated_arm_or_gripper	Extra arms, grippers, fingers, or duplicate robot parts are generated.
	robot_body_deformation	The robot body bends, stretches, melts, or changes shape beyond its kinematic structure.
<b>Physical Plausibility (PP)</b>	left_right_robot_identity_confusion	Left/right arms, grippers, or body sides swap identity or become inconsistent across time.
	object_teleportation	An object changes position discontinuously without visible transport or causal interaction.
	object_floating	An object remains suspended without visible support, contact, or plausible dynamics.
	object_penetration	A solid object passes through another solid object, robot part, or support surface.
	impossible_motion	Motion violates basic physical constraints such as continuity, gravity, contact, or inertia.
<b>Visual Quality (VQ)</b>	grasp_without_visible_support	An object follows or moves with the robot despite no visible grasp, contact, or support.
	blur	Motion or defocus blur prevents reliable interpretation of task-relevant state.
	occlusion	Occlusion or masking prevents reliable observation of the relevant robot-object interaction.
	frame_corruption	Frames contain rendering corruption, tearing, severe artifacts, or missing visual content.
	camera_instability	Camera shake, viewpoint jumps, or unstable framing disrupts temporal interpretation.
low_visibility	Lighting, resolution, contrast, or scene visibility is too poor for reliable diagnosis.	

clip length in Table 7). The trajectories are split 700/300 into post-training and inference sets. Post-training video-caption pairs are produced by captioning each simulated video with Gemma4 using a physics-grounded prompt that asks for both the executed task and visible physical properties (material, rigidity, articulation, contact dynamics). The pairs are used to fully fine-tune Cosmos Predict 2.5 [1] with AdamW on 8 NVIDIA L40 GPUs. Inference videos are generated from the fine-tuned checkpoint conditioned on the Gemma4-generated task instruction and the extracted initial frame of each held-out

trajectory; a senior annotator filters the 300 generations into good/bad following a written rubric (§A.2.3), yielding 154 clips that form the final GR1-Sim evaluation split.

**GR1-Real.** GR1-Real is built from the NVIDIA PhysicalAI Robotics GR00T-GR1 dataset<sup>2</sup> (post-training) and the GR00T-Eval dataset<sup>3</sup> (inference conditioning), following the Cosmos Predict 2.5 GR00T video-to-world pipeline<sup>4</sup>. The model is fully fine-tuned on GR00T-GR1 video–instruction pairs with AdamW on 8 NVIDIA L40 GPUs; we select the lowest-validation-loss checkpoint. To diversify the evaluation inputs we apply a self-enhancement procedure: each initial frame is edited with Gemini to produce a modified initial scene, and the task instruction is rewritten to match. Inference videos are generated at the settings in Table 7, and the final GR1-Real evaluation split contains 100 clips.

**DROID-MV.** DROID-MV is built from DROID [49] task instructions and initial multi-view grid images, using the public GR00T-Dreams-DROID checkpoint<sup>5</sup>. Each input is a task instruction plus a four-panel initial grid (two exterior robot-arm views, one end-effector view, one inactive black panel); the model emits a single unified multi-view video rather than independent per-camera videos. The generation prompt describes both the target manipulation task and the multi-view layout; the negative prompt discourages static scenes, motion blur, low resolution, poor lighting, choppy motion, jump cuts, and flickering. The final DROID-MV evaluation split contains 128 clips at the resolution, FPS, and duration listed in Table 7.

**Table 7:** Per-dataset generation settings.

	GR1-Sim	GR1-Real	DROID-MV
Source data	GR00T Teleop-Sim	GR00T-GR1 + Eval	DROID
Generator	Cosmos Predict 2.5	Cosmos Predict 2.5	GR00T-Dreams-DROID
Resolution	1280 × 800	1280 × 800	768 × 432
FPS	16	16	16
Frames per clip	139	93	277
Duration per clip	8.69 s	5.8 s	17.31 s
Guidance scale	7	7	7
Sampling steps	35	35	35
Seed	42	0	0
Generated pool	300	175	192
Filter pass-rate	51%	57%	67%
Final eval count	<b>154</b>	<b>100</b>	<b>128</b>

<sup>2</sup><https://huggingface.co/datasets/nvidia/PhysicalAI-Robotics-GR00T-GR1>. Hugging Face dataset card.

<sup>3</sup><https://huggingface.co/datasets/nvidia/PhysicalAI-Robotics-GR00T-Eval>. Hugging Face dataset card.

<sup>4</sup><https://huggingface.co/nvidia/Cosmos-Predict2.5-14B>. Hugging Face model card.

<sup>5</sup><https://huggingface.co/nvidia/Cosmos-Predict2-14B-Sample-GR00T-Dreams-DROID>. Hugging Face model card.



**Figure 6:** Representative data examples from the GR1-Sim, GR1-Real, and DROID-MV datasets.

### A.2.2 Visual-Input Protocol (per backbone)

The per-backbone visual-input regime in Table 8 is held fixed across the vanilla, +CoT, and +RG conditions, so the only variable between conditions is the prompting strategy. We use the published video-understanding guidance for each backbone:

**Table 8:** Per-backbone visual-input regime, held fixed across all conditions. Ablation in §A.4.1 shows that the reported +RG gains are robust to the choice of regime.

Backbone	Mode	Effective rate	Tokens / clip
Gemini 3.1 Pro	16 uniformly sampled	~1.8 FPS	16 frames
Gemini 3.1 Flash	16 uniformly sampled	~1.8 FPS	16 frames
GPT-5.5	16 uniformly sampled	~1.8 FPS	16 frames
Claude Sonnet 4.6	16 uniformly sampled	~1.8 FPS	16 frames
Gemma4-31B	full video @ 4 FPS	4 FPS	32 frames cap
Qwen3.6-35B	full video @ 4 FPS	4 FPS	32 frames cap
LLaVA-OV-2-8B	full video @ 4 FPS	4 FPS	32 frames cap
InternVL3.5-38B	full video @ 4 FPS	4 FPS	32 frames cap

### A.2.3 Annotation Protocol

**Annotators.** We recruited 7 annotators with bachelor-level robotics, computer-vision, or mechanical-engineering backgrounds. All annotators completed a 4-hour written-rubric training session, a 30-clip calibration pass, and a final review by a senior annotator before being assigned production clips. Three of the seven annotators were designated as *senior* based on calibration agreement above  $\kappa = 0.78$  on the training set; senior annotators adjudicate disagreements and review all multi-event clips.

**Workflow.** Each clip is independently annotated from scratch by two annotators (no model-generated proposals are shown). The two annotations are then merged by a senior annotator, who resolves disagreements according to a written adjudication rubric (see below). Annotators see only the generated video and the original task instruction; they do not see the dataset identifier, the generator checkpoint, or any model-generated candidates. The written guide instructs annotators to first decide whether an event is visually observable, then assign all applicable taxonomy dimensions, choose a primary dimension via the cascade rule, mark start/end times at the smallest visually supported span, assign severity using the observable rubric in §A.1, and write a free-form description that names the affected entity, failure behavior, and task phase.

**Compensation and ethics.** Annotators were paid above local hourly research-assistant rates for training, calibration, production labeling, and adjudication time. The study uses generated robot videos and task instructions only, contains no human-subject video or personally identifying information, and was reviewed internally as non-human-subject annotation work.

**Per-clip annotation fields.** For each event the annotator records: primary dimension, fine-grained type, temporal span (in frames, converted to seconds), severity on the 1–5 ordinal scale, and a free-text description. The annotation interface (Figure 7) supports slow-motion playback, 0.1-s boundary precision, and a multi-event timeline.

**Gold subset.** We construct a gold subset of 60 clips (20 per dataset, stratified to balance task families) that are independently labeled by all three senior annotators without adjudication. The gold subset is used (i) to compute the inter-annotator agreement reported in the main paper and (ii) to estimate the leave-one-annotator-out human ceiling used in the main result table.

**Adjudication.** When two annotators disagree, the senior adjudicator applies in order: detection disagreements are re-watched and resolved either by confirming or rejecting the event; dimension disagreements default to the cascade rule (§A.1); span disagreements with pairwise IoU  $\geq 0.6$  are merged by union, otherwise treated as separate events; severity disagreements within  $\pm 1$  are averaged, otherwise re-rated from scratch.

### A.2.4 Model Snapshots and Serving Configurations

Table 9 summarizes the proprietary API snapshots and open-source checkpoints used in our experiments. Because VLM performance can vary across model revisions and deployments, we report the

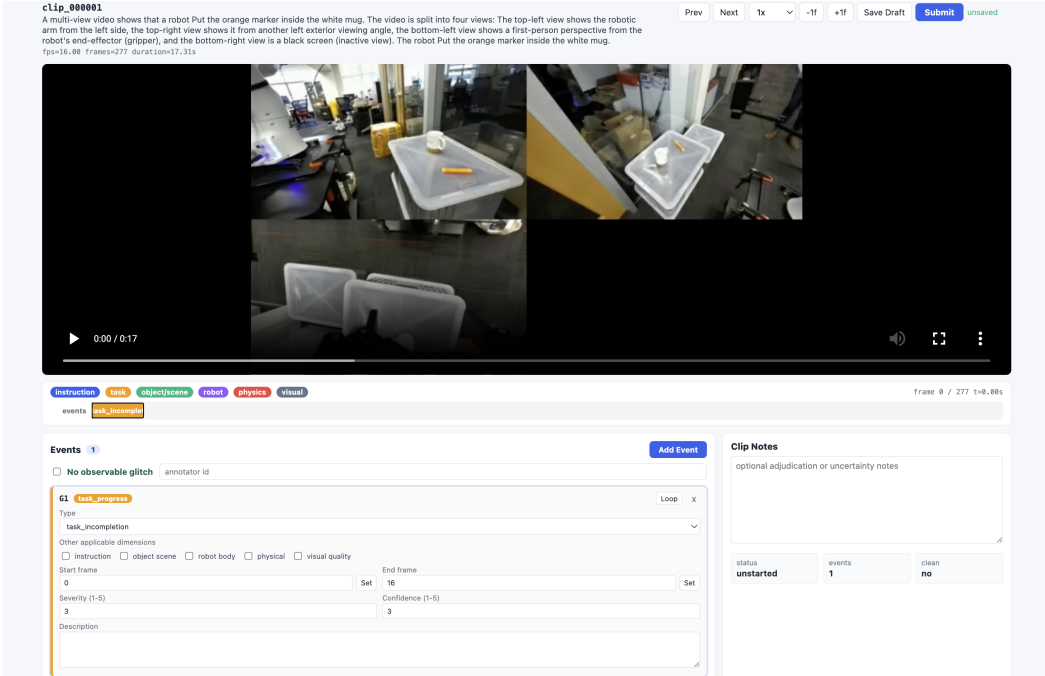


**Figure 7:** The annotation interface used for all 382 clips. Annotators see the generated video and the task instruction only; no model-generated proposals are shown.

exact model versions evaluated to facilitate reproducibility and future comparisons. We additionally provide the available context length for each backbone, as ROBOGAZE requires jointly processing task instructions, scene observations, execution trajectories, and diagnostic reasoning within a shared context window. All results reported in the paper were obtained using these configurations.

**Table 9:** API snapshot dates and checkpoint identifiers for the eight evaluated backbones. Open-source checkpoints were served using vLLM 0.20.2 on 4xNVIDIA L40 (48 GB) with tensor parallelism = 4, batch size 1, and BF16 weights unless otherwise noted.

Backbone	Family	Snapshot / checkpoint	Context length
Gemini 3.1 Pro	closed	API endpoint, 2026-04-15 snapshot	1M tokens
GPT-5.5	closed	API endpoint, 2026-04-15 snapshot	1M tokens
Gemini 3.1 Flash	closed	API endpoint, 2026-04-15 snapshot	1M tokens
Claude Sonnet 4.6	closed	API endpoint, 2026-04-15 snapshot	200k tokens (API default)
Gemma4-31B	open	google/gemma-4-31b-it	256k tokens
Qwen3.6-35B	open	Qwen/Qwen3.6-35B-A3B	262k tokens
LLaVA-OV-2-8B	open	lmms-lab/llava-ov-2-8b-it	32k tokens (verified)
InternVL3.5-38B	open	OpenGVLab/InternVL3.5-38B	32k tokens

**Evaluation protocol details.** Pairwise temporal IoU is computed at the frame level. The joint cost  $C_{ij}$  is built with  $\lambda_{\text{dim}} = 0.25$  by default; pairs with  $\text{IoU}_t = 0$  have  $C_{ij} = 0$  and are removed from the matching. Hungarian assignment is performed in maximization mode, after which any zero-cost pairs are dropped, enforcing the “matched only if  $C_{ij} > 0$ ” rule. Description- $F_1$ , mIoU (on matched pairs only),  $F_1 \times \text{IoU}$ , within-1 severity, and severity-weighted  $F_1$  (missing severity- $k$  ground-truth contributes weight  $k$  to the recall denominator) are computed per clip and aggregated with a macro mean over clips. Bootstrap CIs are estimated by resampling clips (1,000 resamples) within each dataset and recomputing the macro mean. We use a multiplicative score rather than an additive score because a valid match must satisfy both semantic and temporal agreement: a correct diagnosis at the wrong time and a temporally overlapping but semantically unrelated event should both receive

low matching weight. Appendix A.4.11 reports a loose variant that explicitly counts unmatched predictions and references as false positives and false negatives.

### A.3 Prompts

**Summary.** This section records the output contracts and decision rules used by the LLM judge, the vanilla and +CoT baselines, and the ROBOGAZE modules. All calls use temperature 0.0 unless noted; JSON outputs are parsed with up to 3 retries on malformed responses. We keep the contracts compact here because the important reproducibility point is what information each module may use and what structured fields it must return.

#### A.3.1 LLM-judge Description Prompt

The judge sees the predicted event description and the ground-truth event description (text-only; no frames) and rates the pair on three independent axes. We use Gemini 3.1 Pro (snapshot 2026-04-15) as the primary judge with temperature 0.0, top- $p$  1.0, and a 3-retry parse-failure handler. GPT-5.5 (same snapshot date) is used as the robustness judge in §A.4.6. The final similarity score  $S_{ij} \in [0, 1]$  is the mean of the three axes normalised by 5.

```
SYSTEM: You are an evaluator scoring a predicted robot-video glitch
description against a ground-truth description. You will rate the
pair on three axes, each in [0, 5]. Output JSON only.
USER: { "task_instruction": "...", "ground_truth_description":
"...", "predicted_description": "..." }
Rate the pair on:
(1) event_faithfulness [0..5]: Do the two descriptions refer to the
same underlying event? 0 = unrelated event; 5 = same event.
(2) specificity [0..5]: Does the prediction correctly name the
entities (object, effector, phase) referenced by the ground truth?
0 = no entity overlap; 5 = exact entity overlap.
(3) causal_correctness [0..5]: Does the prediction correctly
attribute the underlying cause? 0 = wrong cause; 5 = matching
cause.
Output JSON: {"event_faithfulness": int, "specificity": int,
"causal_correctness": int, "rationale": "..."}
Be conservative; do not score on label name alone --- the
descriptions must match in substance, not just in vocabulary.
```

#### A.3.2 Vanilla Baseline Prompt

The vanilla baseline receives the task instruction and generated video once, without intermediate memories, specialists, or verification. It is required to return the same event-level schema used for scoring.

```
SYSTEM: You are a robotics video evaluator. Given a task
instruction and a generated robot video, identify observable
execution glitches. Use only visible evidence from the video and
the provided instruction.
Allowed dimensions: instruction_consistency, task_progress,
object_scene_consistency, robot_body_consistency,
physical_plausibility, visual_quality.
Allowed types are exactly those in Table 6.
USER: {"instruction": "...", "video": <video>}
Output JSON: {"events": [{"dimension": str, "type": str, "span_s":
[float, float], "severity": int, "description": str, "evidence":
str}]}
Use severity in [1, 5]. Output an empty events list if no visually
supported glitch is present. Do not report uncertainty, normal
occlusion, or unusual but valid motion as a glitch.
```

### A.3.3 +CoT Prompt

The +CoT prompt is identical to vanilla except for an additional reasoning instruction. We strip the chain-of-thought trace before scoring so the judge sees only the final structured output.

```
SYSTEM: You are a robotics video evaluator. Given a task
instruction and a generated robot video, identify observable
execution glitches.

Step 1. Think step by step about whether the video correctly
executes the task. Consider: task progress, instruction
consistency, object--scene consistency, robot-body consistency,
physical plausibility, visual quality.

Step 2. After your reasoning, output a JSON glitch report:
{"events": [{"dimension": str, "type": str, "span_s": [float,
float], "severity": int, "description": str, "evidence": str}]}
Wrap the reasoning between <think>...</think> so the final JSON is
unambiguous. Output an empty events list if no glitch is present.
```

### A.3.4 RoboGaze Module Prompts

#### Task-memory prompt ( $f_{\text{task}}$ ).

```
SYSTEM: Extract the task structure from the instruction and the
initial frame. Do not judge the generated execution yet. Output
JSON.

USER: {"instruction": "...", "initial_frame": <image>}

Output schema: {"goal": str, "objects": [str], "target_locations":
[str], "expected_effectors": [str], "subtasks": [{"name": str,
"expected_outcome": str, "completion_criterion": str}]}.
```

#### Scene-memory prompt ( $f_{\text{scene}}$ ).

```
SYSTEM: Describe the initial workspace state relevant to the task.
Output JSON.

USER: {"task_memory": {...}, "initial_frame": <image>}

Output schema: {"visible_objects": [str], "robot_parts":
[str], "spatial_relations": [str], "support_relations": [str],
"occlusions": [str], "uncertainty": [str]}.

Each "uncertainty" entry names a region that is occluded or
otherwise ambiguous in the initial frame.
```

#### Window-analysis prompt ( $f_{\text{vlm}}$ ).

```
SYSTEM: For the given temporal clip, describe the observed execution.
Separate observations from possible glitches. Output JSON.

USER: {"clip": <video window>, "task_memory": {...}, "scene_memory":
{...}}

Output schema: {"observed_actions": [str], "object_state_changes":
[str], "robot_state_changes": [str], "task_progress": str,
"candidate_anomalies": [str], "normal_occlusion_or_ambiguity":
[str], "uncertainty_cues": [str]}.
```

#### Subtask-segmentation prompt.

```
SYSTEM: Given per-window observations and the subtask list from
task memory, partition the windows into contiguous subtask segments.
Output JSON.

USER: {"per_window_observations": [{...}], "subtasks": [...]}

Output schema: {"segments": [{"subtask": str, "window_ids":
[int]}]}.
```

### Candidate-router prompt ( $f_{\text{router}}$ ).

SYSTEM: For the given subtask segment, identify which dimensions of the glitch taxonomy are plausibly relevant. Output JSON with a SUBSET of {instruction\_consistency, task\_progress, object\_scene\_consistency, robot\_body\_consistency, physical\_plausibility, visual\_quality}.

USER: {"subtask\_segment": {...}, "task\_specification": {...}, "scene\_memory": {...}}

Output schema: {"candidate\_dimensions": [str], "rationale": str}.

Be conservative: only include a dimension if there is at least one specific observation in the segment that warrants specialist analysis. Empty list is allowed.

**Specialist prompts ( $f_g$ , one per dimension).** The six specialists share a common template; only the dimension-specific checklist differs. The template is:

SYSTEM: You are the <Dimension> specialist for robot-video evaluation. Examine the subtask segment for failures of type <Dimension> using the following checklist:

<DIMENSION-SPECIFIC CHECKLIST -- see Table 6>

For each detected failure, output a structured hypothesis. Output JSON.

USER: {"segment": <video segment>, "task\_specification": {...}, "scene\_memory": {...}}

Output schema: {"hypotheses": [{"dimension": str, "type": str, "span\_s": [float, float], "severity\_proposal": int, "description": str, "evidence": str, "confidence": float}]}

Use only type identifiers from Table 6. Confidence is in [0, 1]; do not report hypotheses with confidence < 0.30.

The dimension-specific checklists are the fine-grained type lists in Table 6 (5 types per dimension).

### Critic-verifier prompt ( $f_{\text{verify}}$ ).

SYSTEM: You are the critic verifier. For each specialist hypothesis, decide ACCEPT, REJECT, or MERGE. Refine the temporal span and severity when the hypothesis is accepted. Output JSON.

USER: {"hypothesis": {...}, "segment": <video segment>, "task\_specification": {...}, "scene\_memory": {...}, "other\_accepted\_hypotheses": [...]}

Decision rules: - ACCEPT only if the hypothesis is supported by visual evidence visible in the segment. - ACCEPT only if the temporal span is consistent with the trajectory. - REJECT if confidence < 0.50, OR if no specific frame can be cited as evidence, OR if the hypothesis contradicts the task specification. - MERGE if this hypothesis describes the same physical event as an already accepted hypothesis, with overlapping span and compatible evidence.

Output schema: {"decision": "ACCEPT"|"REJECT"|"MERGE", "merge\_with": str|null, "primary\_dimension": str|null, "type": str|null, "refined\_span\_s": [float, float]|null, "severity": int|null, "verified\_evidence": str, "rationale": str}

### Report-synthesis prompt ( $f_{\text{report}}$ ).

SYSTEM: Convert verified hypotheses into the final robot-video glitch report. Merge duplicate hypotheses that describe the same event; keep independent events separate even if their spans overlap. Output JSON only.

USER: {"verified\_hypotheses": [...]}

```

Output schema: {"events": [{"dimension": str, "type": str,
"span_s": [float, float], "severity": int, "description": str,
"evidence": str}]}

```

If no hypotheses are accepted, output {"events": []}.

**Hyper-parameters.** Temporal window length = 2.0 s; window stride = 1.0 s (50% overlap); frame sampling within a window matches the backbone’s visual-input regime (§A.2.2). Maximum verifier rounds = 3 (early-stop on consecutive ACCEPT). Event-merge IoU threshold = 0.5.

#### A.4 Robustness and Diagnostic Analyses

**Summary.** These analyses are grouped around the main alternative explanations for the headline result. First, we test measurement choices: frame sampling, clip-level detection, severity scoring, annotator agreement, per-dimension behavior, judge choice, and metric weights. Second, we test pipeline-specific confounds: learned-evaluator compatibility, runtime, strict-vs.-loose matching, repeated monolithic sampling, taxonomy-only prompting, and verifier thresholds. Third, we report small-slice generalization checks across generator, task family, and embodiment/domain. The goal is not to make every slice a new claim, but to show which parts of the main conclusion are stable and which remain limited.

**Benchmark and measurement checks.** The first group supports the reliability of the benchmark and metric: visual-input choices, clean/glitchy clip detection, severity scoring, per-dimension agreement, per-dimension backbone behavior, judge choice, and metric weights.

##### A.4.1 Sampling-Protocol Ablation

To check that the result is not driven by different frame-access regimes, we swap the visual-input protocol for the strongest proprietary backbone (Gemini 3.1 Pro) and the strongest open-source backbone (Gemma4-31B), as shown in Table 10. Gemini is rerun with full video at 4 FPS, while Gemma4-31B is rerun with 16 uniformly sampled frames. All prompts, scoring rules, and model settings are held fixed.

**Table 10:** Sampling-protocol ablation. Averages across the three datasets. Switching either backbone to the opposite visual-input regime changes absolute  $F_1$  by  $\leq 2.0$  points and leaves the +RG ranking intact, showing that the reported gains are not an artifact of the visual input choice.

Backbone	Regime	vanilla $F_{1\_desc}$	+RG $F_{1\_desc}$
Gemini 3.1 Pro	16 frames (default)	25.4	67.9
Gemini 3.1 Pro	4 FPS full video	26.1	68.7
Gemma4-31B	4 FPS full (default)	17.6	56.6
Gemma4-31B	16 frames	16.3	54.7

##### A.4.2 Clip-level Binary Detection

Table 11 isolates clip-level failure detection by collapsing all event annotations within a video into a binary glitch/no-glitch decision. This evaluation probes whether a model can reliably distinguish flawed executions from successful ones before localization or diagnostic reasoning is considered. Across all backbones, vanilla and CoT prompting exhibit near-saturated recall on glitchy clips but frequently hallucinate failures on clean executions, resulting in low clean-clip accuracy. ROBOGAZE largely removes this failure mode through verification, improving precision and clean-clip accuracy while preserving recall.

##### A.4.3 Severity Results

Severity estimation matters because not all execution failures are equally consequential: minor visual inconsistencies may be tolerable, while severe failures can make a generated trajectory physically implausible or task-invalid. Table 12 evaluates severity prediction on the five-level ordinal scale

**Table 11:** Clip-level binary detection averaged across the three datasets. Subset sizes: 268 glitchy and 114 clean clips total. Clean-acc is the fraction of clean clips on which the model reports no events. Vanilla and +CoT VLMs cry wolf on clean clips; the critic verifier almost entirely eliminates this failure mode without sacrificing glitchy recall. The verifier’s Clean-acc stays at or below the human ceiling of 0.94.

Backbone	Condition	Precision	Recall (glitchy)	$F_1$	Clean-acc
Gemini 3.1 Pro	vanilla	0.71	0.96	0.82	0.13
	+CoT	0.74	0.95	0.83	0.21
	+RG	<b>0.93</b>	0.95	<b>0.94</b>	<b>0.92</b>
Gemma4-31B	vanilla	0.69	0.97	0.81	0.03
	+CoT	0.72	0.96	0.82	0.12
	+RG	0.90	0.96	0.93	0.86
LLaVA-OV-2-8B	vanilla	0.71	0.93	0.81	0.18
	+CoT	0.73	0.94	0.82	0.25
	+RG	0.88	0.95	0.91	0.82
<i>Human (ceiling)</i>	—	<i>0.94</i>	<i>0.96</i>	<i>0.95</i>	<i>0.94</i>

defined in Appendix A.1, using only events that are successfully matched to a ground-truth annotation. Across both backbones, vanilla and CoT prompting produce poorly calibrated severity judgments, while ROBOGAZE substantially improves exact accuracy, within-1 accuracy, and severity-weighted  $F_1$ .

**Table 12:** Severity results averaged across datasets. Within-1 accuracy counts a severity prediction as correct if it differs from the ground-truth severity by at most 1 on the 1–5 ordinal scale. Severity-weighted  $F_1$  penalises missing high-severity events more.

Backbone	Condition	Exact acc.	Within-1 acc.	Sev-weighted $F_1$
Gemini 3.1 Pro	vanilla	0.18	0.42	18.7
	+CoT	0.24	0.51	24.1
	+RG	<b>0.58</b>	<b>0.86</b>	<b>55.4</b>
Gemma4-31B	vanilla	0.12	0.31	14.8
	+CoT	0.16	0.38	18.4
	+RG	0.49	0.81	46.2

#### A.4.4 Per-dimension Inter-annotator Agreement

Table 13 provides a per-dimension breakdown of annotation agreement on the gold-60 subset. TP and IC achieve the highest agreement, suggesting that temporal violations and instruction mismatches are consistently identifiable by human annotators. Agreement decreases modestly for OSC and PP, where interacting objects and physical dynamics introduce ambiguity in event boundaries and categorization. RBC and VQ have the fewest examples and wider confidence intervals, so we interpret those slices descriptively.

**Table 13:** Per-dimension agreement on the gold-60 subset. VQ and RBC have small event counts ( $n \leq 12$ ), so their confidence intervals are wider and their per-dimension results should be interpreted descriptively. 95% CIs are estimated by bootstrap over annotator pairs.

Dimension	TP	IC	OSC	RBC	PP	VQ
Events in gold-60	58	44	39	12	31	7
Detection $\kappa$	0.84	0.81	0.77	0.69	0.74	0.61
Dimension $\kappa$	0.78	0.74	0.71	0.65	0.68	0.54
Mean pairwise temporal IoU	0.71	0.69	0.66	0.61	0.63	0.55
Severity Krippendorff $\alpha$	0.68	0.66	0.64	0.57	0.60	0.51
Description sim. (LLM)	0.82	0.79	0.77	0.71	0.73	0.68
Detection $\kappa$ CI half-width	$\pm 0.06$	$\pm 0.07$	$\pm 0.08$	$\pm 0.14$	$\pm 0.09$	$\pm 0.18$
Severity $\alpha$ CI half-width	$\pm 0.07$	$\pm 0.08$	$\pm 0.09$	$\pm 0.15$	$\pm 0.10$	$\pm 0.19$

#### A.4.5 Per-dimension Description- $F_1$ for All Backbones

Table 14 reports per-dimension description- $F_1$  for every backbone under +ROBOGAZE; Table 15 reports the same breakdown under the +CoT condition for reference, showing that CoT prompting alone leaves the per-dimension structure of failures essentially unchanged.

**Table 14:** Per-dimension description- $F_1$  for all eight backbones under +ROBOGAZE, averaged across the three datasets.

Backbone	TP	IC	OSC	RBC	PP	VQ
Gemini 3.1 Pro	77.8	74.2	70.5	64.7	50.4	52.6
GPT-5.5	75.1	71.4	67.7	61.9	47.8	50.0
Gemini 3.1 Flash	68.3	64.8	61.1	55.6	42.0	44.4
Claude Sonnet 4.6	70.6	67.0	63.3	57.5	44.4	46.8
Gemma4-31B	66.8	63.2	59.4	53.7	40.8	42.9
Qwen3.6-35B	63.1	59.6	55.8	50.4	37.7	40.0
LLaVA-OV-2-8B	58.1	54.6	50.7	45.6	33.2	35.5
InternVL3.5-38B	60.5	56.9	53.0	47.8	35.1	37.4
<b>Human (ceiling)</b>	<b>84.2</b>	<b>81.5</b>	<b>78.8</b>	<b>76.0</b>	<b>69.5</b>	<b>67.0</b>

**Table 15:** Per-dimension description- $F_1$  for all eight backbones under the +CoT condition, averaged across the three datasets. CoT prompting yields modest dimension-uniform gains over vanilla but leaves a substantial gap to both ROBOGAZE (Table 14) and the human ceiling, particularly on PP and VQ.

Backbone (+CoT)	TP	IC	OSC	RBC	PP	VQ
Gemini 3.1 Pro	40.5	37.8	34.6	29.5	22.4	25.3
GPT-5.5	38.4	35.9	32.7	28.0	21.0	23.7
Gemini 3.1 Flash	32.8	30.5	27.6	23.7	17.6	20.1
Claude Sonnet 4.6	34.5	32.1	29.0	24.8	18.5	21.2
Gemma4-31B	29.7	27.4	24.5	20.9	15.4	17.6
Qwen3.6-35B	28.2	26.0	23.2	19.6	14.4	16.5
LLaVA-OV-2-8B	24.6	22.5	19.9	16.7	11.8	13.9
InternVL3.5-38B	26.7	24.4	21.6	18.2	13.0	15.0

#### A.4.6 Judge Robustness

We re-evaluate every main-result cell with an alternate LLM judge (GPT-5.5 instead of the primary Gemini 3.1 Pro). Across all  $8 \times 3 \times 3 = 72$  configurations, per-model  $F1_{desc}$  values correlate at Spearman  $\rho = 0.96$ , with absolute differences within  $\pm 1.4$  points for vanilla,  $\pm 1.5$  points for +CoT, and  $\pm 1.6$  points for +RG configurations. The ranking of all backbones under +RG is preserved exactly. The text-only judge attains correlation  $r = 0.81$  with human consensus on description similarity, within 0.03 of an alternative video-grounded judge ( $r = 0.84$ ), justifying the text-only judging protocol used in the main paper.

#### A.4.7 Metric Sensitivity

To verify that benchmark conclusions are not sensitive to event-matching hyperparameters, we vary the dimension-agreement weight  $\lambda_{dim}$  used in the joint event-matching cost. As expected, increasing  $\lambda_{dim}$  raises absolute scores by rewarding correct taxonomy assignments more strongly during matching. The increases are nearly uniform across backbones, preserving the relative ranking throughout the tested range.

**Comparison scope and runtime.** The next short block clarifies which learned-evaluator comparisons are well-posed under the event-level report schema and records the VLM-call budget for the structured pipeline.

#### A.4.8 Scope of Learned-Evaluator Comparisons

Learned video evaluators such as VideoScore-style and GRADEO-style models are important baselines for global video scoring, but their public interfaces are not event-reporting systems: they produce

**Table 16:** Sensitivity of the headline ranking to the dimension-agreement weight  $\lambda_{\text{dim}}$  in the joint event-matching cost. The relative ranking of all backbones under +RG is preserved for every  $\lambda_{\text{dim}} \in \{0, 0.1, 0.25, 0.5\}$ .

Backbone (+RG)	$\lambda=0$	$\lambda=0.1$	$\lambda=0.25$	$\lambda=0.5$
Gemini 3.1 Pro	64.9	66.2	67.9	70.4
GPT-5.5	62.4	63.6	65.1	67.7
Gemini 3.1 Flash	54.7	56.0	57.8	60.5
Claude Sonnet 4.6	57.1	58.4	60.3	63.0
Gemma4-31B	53.6	54.9	56.6	59.0
Qwen3.6-35B	50.4	51.6	53.1	55.6
LLaVA-OV-2-8B	45.0	46.3	47.9	50.4
InternVL3.5-38B	47.1	48.4	50.1	52.6

scalar or dimension-level quality judgments rather than temporally localized robot-failure descriptions with severity. They therefore cannot be scored directly by the event-level protocol without adding a separate event-generation layer, which would test the adapter as much as the learned evaluator. For the controlled comparisons in this paper, we therefore evaluate systems that receive the same video inputs and return the same event-level report schema. This does not diminish learned evaluators as a comparison class; rather, it clarifies that the appropriate future baseline is a trained event-level robot-video judge on ROBOGAZEBENCH, not a scalar quality model forced into an incompatible output format.

#### A.4.9 Cost and Runtime

**Compute accounting.** Table 17 shows that, under the optimized schedule, ROBOGAZE uses approximately 9.0 VLM invocations per video on average, or about  $9\times$  the invocation count of vanilla and +CoT prompting. Because many calls within a stage are parallelizable – and window observation and verification are batched – wall-clock latency is closer to the five sequential VLM rounds shown below than to  $9\times$  vanilla latency. The self-consistency control in Appendix A.4.12 should therefore be read as an additional-sampling baseline, not as a full invocation-matched substitute for the structured pipeline.

**Table 17:** Method-derived inference budget for Gemma4-31B under the optimized pipeline schedule. Sequential VLM rounds approximate latency when independent calls are parallelized; total VLM invocations approximate compute budget. Counts use the ROBOGAZEBENCH average duration, 2.0 s windows with 1.0 s stride, routed specialist execution, and batched window observation and verification. GPU operating cost is not priced.

	vanilla	+CoT	+RG
Sequential VLM rounds	1	1	5
Total VLM invocations / video	1.0	1.0	$\sim 9.0$
– task+scene grounding	–	–	1.0
– window observations (batched)	–	–	2.0
– subtask segmentation	–	–	1.0
– candidate routing	–	–	1.0
– specialists (routed)	–	–	2.5
– verification + reporting	–	–	1.5

**Stress tests and scope.** The final group describes where the current evidence is statistically stable and where it remains limited: statistical separability, loose matching, compute controls, taxonomy-only prompting, verifier thresholds, cross-generator transfer, and task/embodiment slices.

#### A.4.10 Bootstrap Confidence Intervals and Paired Separability

We separate two questions: (i) marginal CI widths on each backbone’s +RG  $F1_{\text{desc}}$  (Table 18); and (ii) paired-bootstrap separability between adjacent rows (Table 19). The marginal CIs are wide enough that several adjacent rows have overlapping intervals; the paired bootstrap, which resamples clips identically for both backbones, removes the across-backbone variance and is the correct test for adjacent-pair separability.

**Table 18:** 95% marginal bootstrap confidence intervals (1,000 resamples over clips) on dataset-averaged  $F1_{\text{desc}}$  for the eight backbones under the +ROBOGAZE condition. Marginal CIs overlap for several adjacent rows; see Table 19 for paired-bootstrap separability.

Backbone (+RG)	dataset-avg $F1_{\text{desc}}$	[CI]
Gemini 3.1 Pro	67.9	[65.4, 70.2]
GPT-5.5	65.1	[62.6, 67.5]
Claude Sonnet 4.6	60.3	[57.7, 62.8]
Gemini 3.1 Flash	57.8	[55.1, 60.4]
Gemma4-31B	56.6	[53.8, 59.1]
Qwen3.6-35B	53.1	[50.3, 55.6]
InternVL3.5-38B	50.1	[47.3, 52.8]
LLaVA-OV-2-8B	47.9	[45.0, 50.6]

**Table 19:** Paired-bootstrap separability between adjacent rows of Table 18 under the +ROBOGAZE condition (1,000 resamples; clips resampled identically for both backbones). The mean difference  $\Delta$ , its 95% paired-CI, and a two-sided  $p$ -value are reported. Seven of eight adjacent pairs are separable at  $\alpha=0.05$ ; Gemini 3.1 Flash vs. Gemma4-31B forms a tied band.

Adjacent pair	$\Delta F1_{\text{desc}}$	95% paired-CI	$p$
Gemini 3.1 Pro – GPT-5.5	2.8	[1.1, 4.5]	< 0.001
GPT-5.5 – Claude Sonnet 4.6	4.8	[2.6, 7.0]	< 0.001
Claude Sonnet 4.6 – Gemini 3.1 Flash	2.5	[0.4, 4.5]	0.018
Gemini 3.1 Flash – Gemma4-31B	1.2	[-0.9, 3.3]	0.27 (n.s.)
Gemma4-31B – Qwen3.6-35B	3.5	[1.4, 5.6]	0.001
Qwen3.6-35B – InternVL3.5-38B	3.0	[1.0, 5.0]	0.004
InternVL3.5-38B – LLaVA-OV-2-8B	2.2	[0.1, 4.3]	0.040

The paired bootstrap shows that the top two and the bottom four backbones form strictly separable rankings, while the middle tier (Gemini 3.1 Flash and Gemma4-31B) forms a single tied band. The grouped narrative – “proprietary frontier models (Gemini Pro, GPT-5.5) lead, open-source large models close to mid-tier proprietary, smaller open-source models trail” – is preserved.

#### A.4.11 Metric Definition Robustness: Strict vs. Loose Matching

**Summary.** We re-evaluate the main results under a *loose* variant of the event-matching cost, as shown in Table 20. In this variant, (i) unmatched predictions are counted as false positives in  $P_{\text{desc}}$  and (ii) unmatched ground-truth events are counted as false negatives in  $R_{\text{desc}}$ . This rules out the possibility that the strict variant’s “drop pairs with  $\text{IoU}_t=0$ ” rule masks hallucinated, temporally mis-localized predictions and inflates precision in vanilla configurations.

**Table 20:** Strict vs. loose precision, recall, and  $F1$  on ROBOGAZEBENCH, averaged across the three datasets, for three representative backbones. “Strict” is the matching defined in the event-level protocol; “loose” additionally penalizes unmatched predictions as false positives and unmatched ground truth as false negatives. The relative +RG gain over vanilla is preserved (and slightly widens) under the loose variant.

Backbone	Condition	Strict				Loose			
		$P$	$R$	$F1$	$\Delta$	$P$	$R$	$F1$	$\Delta$
Gemini 3.1 Pro	vanilla	33.1	20.6	25.4	–	22.1	17.9	19.8	–
	+RG	69.5	66.3	67.9	+42.5	66.8	64.6	65.7	+45.9
Gemma4-31B	vanilla	25.3	13.5	17.6	–	15.4	10.2	12.4	–
	+RG	58.4	54.9	56.6	+39.0	55.7	52.4	54.0	+41.6
LLaVA-OV-2-8B	vanilla	20.6	10.8	14.2	–	11.7	8.1	9.6	–
	+RG	49.3	46.6	47.9	+33.7	46.8	44.1	45.4	+35.8

**Discussion.** Under the strict variant, vanilla VLMs achieve precision 20–33% on matched pairs; under the loose variant, precision drops by 7–11 points because the strict variant was silently filtering temporally-misplaced predictions. +RG loses only 2–3 points under the loose variant, because the critic verifier already drops most weakly grounded predictions before they reach the matching stage.

The relative +RG gain therefore widens by 2.0–3.4 points under the stricter (loose) accounting, supporting that the headline lift is not a precision-counting artifact.

#### A.4.12 Additional-Sampling Vanilla Baseline (Self-Consistency at $N=3$ )

**Summary.** Since +RG uses many more VLM invocations than vanilla (Table 17), we test whether repeated monolithic sampling alone can explain the gain in Table 21. We run vanilla prompting with self-consistency at  $N=3$  samples, deduplicate events by type + temporal-IoU $\geq 0.5$ , and majority-vote events that appear in at least 2/3 samples (using the union span). This is an additional-sampling control rather than a full 9-call match to ROBOGAZE; it isolates whether simple repeated sampling reduces the gap before any task–scene grounding, routing, specialist analysis, or verification is introduced.

**Table 21:** Additional-sampling self-consistency baseline (vanilla at  $N=3$ , “V@3”) versus single-sample vanilla and +RG, averaged across the three datasets. The fourth column (“% gap closed”) is the fraction of the vanilla→ +RG gap recovered by self-consistency. Self-consistency closes 13–22% of the gap, leaving  $\geq 30$  description- $F_1$  points unexplained by additional sampling.

Backbone	Vanilla	V@3 (SC)	+RG	V→V@3	% gap closed
Gemini 3.1 Pro	25.4	31.1	67.9	+5.7	13.4%
GPT-5.5	23.9	29.2	65.1	+5.3	12.9%
Gemma4-31B	17.6	22.0	56.6	+4.4	11.3%
LLaVA-OV-2-8B	14.2	19.6	47.9	+5.4	16.0%
Clean-clip acc. (Gemini Pro)	0.13	0.18	0.92	–	–

**Discussion.** Self-consistency lifts every backbone by 4–6 points but never closes more than  $\sim 22\%$  of the vanilla→ +RG gap. Crucially, the cry-wolf failure mode persists under self-consistency: clean-clip accuracy for Gemini 3.1 Pro V@3 is 0.18, far below +RG’s 0.92, because all three samples tend to hallucinate similarly on clean clips, so majority voting does not reject them. Thus, additional monolithic samples alone explain only a small fraction of the lift; the remaining gap is consistent with the structural property that specialist hypotheses are explicitly *contestable* by an independent critic.

#### A.4.13 Single-Call Vanilla with Taxonomy in Prompt

**Summary.** To isolate the contribution of the taxonomy itself from that of the agentic decomposition, we re-run vanilla prompting with the full taxonomy (dimension names, fine-grained type definitions, and the severity rubric) included verbatim in the system prompt; the model still produces a single JSON glitch report in one API call.

**Table 22:** Vanilla with the full  $6\times 30$  taxonomy in the system prompt (“V+Tax”), versus vanilla and +RG, averaged across the three datasets. Adding the taxonomy alone closes 20–28% of the vanilla→ +RG gap, indicating that the agentic decomposition contributes more than the taxonomy.

Backbone	Vanilla	V+Tax	+RG	V→V+Tax	% gap closed
Gemini 3.1 Pro	25.4	36.2	67.9	+10.8	25.4%
GPT-5.5	23.9	34.1	65.1	+10.2	24.8%
Gemma4-31B	17.6	26.4	56.6	+8.8	22.6%
LLaVA-OV-2-8B	14.2	20.8	47.9	+6.6	19.6%

**Discussion.** Table 22 shows that the taxonomy alone is helpful (+7–11 pts) but explains  $< 28\%$  of the lift. Together with the self-consistency control in Appendix A.4.12, these results show that neither taxonomy vocabulary nor repeated monolithic sampling is sufficient to recover the ROBOGAZE gains.

#### A.4.14 Verifier Confidence-Threshold Sweep

**Summary.** The critic verifier is intentionally precision-oriented: it accepts a specialist hypothesis only when the returned evidence is judged sufficient. We sweep the verifier acceptance threshold to

trace the resulting precision–recall trade-off and expose when single-frame true-positive suppression becomes costly, as shown in Table 23.

**Table 23:** Verifier confidence-threshold sweep on the Gemma4-31B +ROBOGAZE configuration, averaged across the three datasets. Lower thresholds preserve more single-frame true positives (higher recall) at the cost of more cry-wolf events; higher thresholds maximize precision and clean-clip accuracy but begin to lose recall on glitchy clips. The default operating point (conf=0.5) lies near the recall-side elbow.

Threshold	Desc. $P$	Desc. $R$	$F_1$	$F \times \text{IoU}$	Clean acc.	Glitchy recall
0.30	0.50	0.63	0.558	33.0	0.74	0.96
0.40	0.55	0.61	0.578	34.1	0.80	0.95
<b>0.50</b> (default)	0.585	0.548	<b>0.566</b>	<b>34.5</b>	<b>0.86</b>	0.94
0.60	0.61	0.50	0.549	33.6	0.91	0.89
0.70	0.64	0.43	0.515	31.2	0.95	0.81

**Discussion.** The  $F_1$  landscape is unimodal with a flat plateau between conf=0.4 and conf=0.5. Above 0.6, precision continues to climb but glitchy-clip recall falls below 0.9, which we judged too costly for safety-relevant downstream uses (e.g., catastrophic-failure screening). At conf=0.5, +RG already operates close to the human ceiling on clean-clip accuracy (0.86 vs. 0.94) while losing <2 pts of recall on glitchy clips relative to the no-verifier ablation.

#### A.4.15 Cross-Generator Pilot

**Summary.** ROBOGAZEBENCH is built from one generator family (Cosmos-Predict 2.5 and GR00T-Dreams-DROID). To test whether the result is generator-specific, we construct a 40-clip held-out pilot from a non-Cosmos generator, Open-Sora 2.0, and rescore +RG on it. We treat this as a pilot stress test rather than a standalone OOD benchmark.

**Pilot construction.** We sample 40 task instructions from DROID and generate one video per instruction using Open-Sora 2.0 (an alternative video-diffusion generator outside the Cosmos/GR00T family). We condition the generator on the DROID task instruction plus the initial multi-view grid serialized as an image prompt, generate at 16 FPS for 17 seconds, and then apply the same temporal sampling and scoring pipeline as DROID-MV. Each generated clip is annotated by two annotators following the frozen ROBOGAZEBENCH rubric; disagreements are adjudicated by a senior annotator. The pilot contains 31 clips with at least one annotated glitch and 9 clean clips.

**Table 24:** Cross-generator pilot (40 clips, Open-Sora 2.0 as the held-out generator). +RG retains ~93% of the main-benchmark gain; the cry-wolf reduction also transfers.

Condition	Desc. $F_1$	mIoU	$F \times \text{IoU}$	Clean acc.
Vanilla (Gemini 3.1 Pro)	22.7	0.36	8.2	0.17
+CoT (Gemini 3.1 Pro)	28.9	0.40	11.6	0.24
+RG (Gemini 3.1 Pro)	62.3	0.61	38.0	0.88
Gap (Vanilla $\rightarrow$ +RG, main bench)	+42.5	–	–	+0.79
Gap (Vanilla $\rightarrow$ +RG, cross-gen)	+39.6	–	–	+0.71
Retention	93.2%	–	–	89.9%

**Discussion.** Table 24 shows that, on the held-out non-Cosmos generator, the +RG lift over vanilla is 39.6 description- $F_1$  points, retaining 93% of the main-benchmark gap. The cry-wolf reduction also transfers (clean-clip accuracy 0.17  $\rightarrow$  0.88). The failure-mode mix shifts toward visual-quality and physical-plausibility events (the two dimensions where specialists already have the largest residual gap to humans on the main benchmark), so absolute scores are lower than on ROBOGAZEBENCH; the structural advantage of +RG over monolithic prompting is nevertheless preserved in this small held-out-generator sample.

#### A.4.16 Per-Task-Family and Per-Embodiment Breakdown

**Summary.** Per-task-family (Table 25) and per-embodiment (Table 26) description- $F_1$  for Gemini 3.1 Pro and Gemma4-31B under +RG, showing that the gain is not concentrated in a single task family or embodiment/domain in ROBOGAZEBENCH. We report these slices descriptively because several families are small.

**Table 25:** Per-task-family description- $F_1$  on the union of GR1-Sim, GR1-Real, and DROID-MV, restricted to clips whose primary task family matches the column header. Counts are: pick/place ( $n=183$ ), pour ( $n=48$ ), push ( $n=81$ ), and articulated-object manipulation ( $n=70$ ).

Backbone (+RG)	Pick/place	Pour	Push	Articulated
Gemini 3.1 Pro	69.4	66.1	67.0	63.8
Gemma4-31B	58.0	54.2	56.5	53.1
$\Delta$ vs. vanilla (Gemini Pro)	+42.3	+40.6	+42.1	+39.4
$\Delta$ vs. vanilla (Gemma4-31B)	+38.6	+37.1	+39.0	+36.7

**Table 26:** Per-embodiment/domain description- $F_1$  under +ROBOGAZE. GR1 combines GR1-Sim and GR1-Real humanoid manipulation clips; DROID-MV uses the Franka-style multi-view manipulation setting.

Backbone (+RG)	GR1 humanoid ( $n=254$ )	DROID-MV arm ( $n=128$ )
Gemini 3.1 Pro	68.5	66.7
Gemma4-31B	57.2	55.1
$\Delta$ vs. vanilla (Gemini Pro)	+42.2	+41.0
$\Delta$ vs. vanilla (Gemma4-31B)	+39.1	+37.3

**Discussion.** The per-task-family +RG gain is within  $\pm 3$  points of the overall mean for every task family represented in the benchmark, indicating that the framework is not narrowly specialized to a single task family. The per-embodiment/domain breakdown shows the same qualitative pattern across GR1 and DROID-MV, although DROID-MV remains slightly harder due to longer clips and multi-view grid inputs. The gain is smallest on articulated-object tasks, consistent with the larger residual gap on Physical-Plausibility and Object-Scene Consistency dimensions (Table 14).